博士論文

Doctoral Thesis

Improvement of Back–drivability for Geared Two–inertia System
ギア付き二慣性システムのためのバックドライバビリティの向上

指導教官　下野 誠通 准教授

Associate Professor　Tomoyuki Shimono

2020 年 6 月提出

June, 2020

横浜国立大学大学院　工学府 物理情報工学専攻

電気電子ネットウーク　コース

Division of Physics, Electrical and Computer Engineering

Graduate School of Engineering, Yokohama National University

15SD191 徐　爽

Shuang Xu

Abstract

This thesis presents the improvement of back–drivability based on geared two–inertia system. Gear reduction is widely used in a lot of mechatronic systems, because of its benefit of increasing torque even in the limited condition of room, mass, and motor capacity. According to the increasing demand of force control applications to realize flexible interaction between system and environment, it is also expected that geared motors to be utilized in force or torque control applications.

Back–drivability is the ability for interactive transmission of force between input and output, especially from the external torque of load side to the acceleration of motor. The robots for those applications need to be achieved safety contact with objects and environments are more required. However, in geared system, there is a serious problem that the back–drivability becomes low due to introduction of inertia, friction, backlash, and noise.

Considering the characteristic of a geared motor system, back driving is more difficult than forward driving. Back–drivability can be improved if it can be transformed to a driving of forwarding motion. This thesis also focuses on this target based on the point of view of inertia transformation. Moreover, the back–drivability is a sensitive index of force transmission from the load terminal to the motor output. If the estimated input torque from the load terminal goes through the controller, which can design back–driving inertia equivalently, an adjustable sensitivity of transmission will be realized to achieve better performance of the back–drivability.

Technically, this thesis proposes an improvement method of back–drivability in torque control. The method is based on Disturbance Observer (DOB) and Load–side Disturbance Observer (LDOB). A disturbance observer realizes robust motion control and load–side disturbance observer estimates a load–side torque input. The proposed method modifies the characteristics of back-drivability by implementing a designed controller to achieve scaled back–drivability based on referenced forward–drivability.

In experiments, both conventional method and proposed control method are actually implemented in different conditions. The effectiveness of proposed method is clarified by comparing to conventional experiment results. Back–drive can achieve as same level drivability as forward–drive, and also can achieve quantified improvement of back–drivability by adjusting scaling factor.

Overall, the proposed control method not only can easily to apply to human support system, human–robot interaction and so on to achieve safety based on high–drivability demand, but also can support the applications of rehabilitating exercises that required a robot with adjustable back–drivability for different rehabilitation courses based on different physically handicapped person. So, wide range of back–drivability can help robot to adapt to different applications.

Table of Contents

List of Figures

List of Tables

Chapter 1

Introduction

1.1 Background

Recently, Comparing to the conventional industrial manipulators, the robots for those applications need to be achieved safety contact with objects and environments are more required. An actuator which can be back–driven when applies an external force to the output of the actuator, and it causes the actuator drive mechanism to move is one of the evaluation criteria. The most common example that is not back–drivable is a worm gear setup [1]. The determination of back–drivability for an actuator system is mostly the angles that force conversion takes as it moves through the system.

Back–drivability is the ability for interactive transmission of force between input and output [2], especially from the external torque of load side to the acceleration of motor [3]. Unlike traditional industry robots, the novel mechanical designed robot arm, which is applied with the series elastic actuator (SEA) [4] retaining high back–drivability, allows people to move the terminal of the arm to the target point directly. SEAs have been successfully applied in numerous scenarios for more than 20 years even if It is hard to adopt direct–drive motors [5], elastic actuators [6]. However SEAs as passive flexible actuator with complicated structure and difficult control demand, normally connects to a rigid motor system which retains uncontrollable stiffness. Other active actuators usually need to implement force sensor [7] in the terminal to detect the force or torque which is given by people.

Another problem is that introduction of the elastic element reduces the actuator bandwidth and makes position control difficult [8]. Moreover, it is prone to vibrate, which deteriorates system stability and requires extra power for position control [9]. Several approaches have been proposed to control the position of elastic-joint robots. Kim et al. [10] proposed a robust PD control scheme for flexible-joint robots based on a DOB which was only applied to the motor-side dynamics.

Geared two–inertia system has been widely used in various kinds of mechatronic systems, since the operation range could be adjusted by reduction ratio to overcome the limitation of output velocity and torque in required conditions, such as room, mass, and motor capacity. Not only precise position control, but also torque control applications in geared two–inertia system are required. In force and torque control applications [11, 12, 13], it is expected to realise soft interaction between system and environment. The combination of geared two–inertia system and back–drive suppose to have wide prospect applications such as medical robot [14] and friendly humanoid robot for micro–invasive surgery [15].

1.2 Conventional approaches based on problems

Gears introduce inertia, friction, backlash, and noise. They also make the back–drivability of motor low. The obvious drawback of them is that the contact friction at gear teeth is large and the viscous friction. A lot of researches focus on the friction compensation of geared system to improve the back–drivability such as [16, 17, 18, 19] through the torque sensor to create the accurate model of friction. There is also some authors try to compensate the friction of system by the feed–forward or feed–back control [20]. In all of the above methods, it attempts to compensate frictions for the system by finding an accurate frictional model, which in turn improves back–drivability. However, they all require accurate system parameter identification through established frictional models, and not only the identification process is complex, but for some applications with complex mechanical structure, parameter identification is almost impossible.

Back–drive inertia is also a reason to make back–drivability low. Inertia is the property of an object of matter to resist change in acceleration. The more inertia it has, the more force will be required to change the acceleration of that object. Some researchers have also proposed some methods which discuss the back–drivability of motor system itself to improve its performance by controller of combination of P and I [21], joint torque and backlash [22]. The referenced method [21] offers a control method that is controlled by simple, easily portable controllers, which will be comprehensive compared with the proposed method presented in this thesis in later. The referenced method [22] takes advantage of the nature disadvantage of the gear motor itself such as backlash, and obtains a relatively ingenious way to improve back–drivability. But this method can only be used for back drive motion, which is to achieve good performance of back–drivability by sacrificing forward drive motion, so it is not suitable for applying to other applications. A geared two–inertia system which is mostly utilised in industrial robots is discussed in Reference [23], which is shown that the vibration can be suppressed by controlling the ratio between resonant and anti–resonant frequencies via spring torque feedback gain for

two–mass system. In this method, there is no emphasis on compensation for accurate vibration suppression for flexibly connected two–mass system, but it provides a design thinking based on the physical characteristics of the gearbox system itself, even if it is not about improvement of back–drivability.

Robustness is essential to design a high-performance motion control system in practice. Disturbance Observer (DOB) [24] which estimates external disturbances and system uncertainties, such as external load, friction, inertia variation is widely used to achieve the robustness of motion control systems for the sake of its simplicity and efficiency [25, 26]. The bandwidth of DOB is directly related to the robustness of the motion control system. The higher the bandwidth of DOB is, the more robustness can be expected. It should be noted that the actual bandwidth of DOB is limited by practical constraints such as noise, sampling time [27].

The external disturbance of load side can be estimated to apply for torque semi–closed loop control because of Load–side Disturbance Observer (LDOB) [28]. In conventional torque control in geared two–inertia system, the combination of different controller and disturbance observer [29], load–side observer and motor–load disturbance observer are proposed. No matter what kind of the combinations of each other, it is normally composed of two parts such as the observers for information collection and the controllers for control performance. In deeply the role of each disturbance observer plays in back–driving control system need to clarified. A combination of observers for drive motor and load are also used in this research. In this thesis, the combination that can simplify the calculation as far as possible is used to avoid the need for precise parameters, which can improve the adaptability of this design system.

1.3 Target of Research

The back–drivability of geared two–inertia system is an important characteristic which needs to be clarified. Considering the characteristic of a geared motor system, back–driving is more difficult than forward–driving. Back–drivability can be improved if it can be transformed to a driving of forwarding motion [30]. This thesis also focuses on this target based on the position of inertia transformation. Moreover, the back–drivability is a sensitive index of force transmission from the load terminal to the motor output. If the estimated input torque from the load terminal goes through the controller which can design back–driving inertia equivalently, an adjustable sensitivity of transmission will be realised to achieve better performance of the back–drivability.

According to above structures of disturbance observer and load–side disturbance observer, the introduced scaled controller for designed back–drivability control, an adjustable back–drivability could satisfy requirements for kinds of applications.

1.4 Composing of this Thesis

This thesis is organised as follows. The following chapter 2 expresses the geared two–inertia system and conception of equivalent back–drive inertia of system. The experimental equipment and supporting components based on this control model used in the thesis are also described in detail. The typical conventional control method is discussed to illustrate the characteristics and advantages of the control components used in this thesis in chapter 3. Strategy of torque control for improving back–drivability, and where the controller's parameters are imputed and frequency characteristics and step response analysis are discussed in chapter 4 and chapter 5. In chapter 6, the discrete controller $H(s)$ is present to give the design of scaling factor that applied to experimental environment. The stability analysis and feature of scaling factor α are discussed chapter 7.The last, the discussed control methods is compared by experiments in chapter 8. The adjustable back–drivability of proposed method is also realised by α. Finally, the summary of this paper is described in chapter 9.

Chapter 2

Control model: Geared two–inertia system

2.1 Introduction

In this chapter, the mechanical structure of a geared two–inertia system is introduced and shown. The mechanical formulas for motion control is described based on the block diagram of geared two–inertia system. According to it, the conception of equivalent inertia from angular acceleration of motor to torque is explained. Then in detail, the equivalent forward–drive inertia and back–drive inertia of geared two–inertia system are mathematically discussed to show the deterioration of back–drive inertia. The concept of back–drivability is also clarified in mathematics.

2.2 Structure of geared two–inertia system

In this section, the kinematics of system including geared connection between motor and load is presented. The schematic view of modelling is shown as Fig. 1. The motor connected with gearbox generates decelerated angular velocity $\dot{\theta}_l$ and increased output torque τ_l. The decelerating and increasing ratio is associated with gearbox G_r. As known common mechanical formulas as follow Eq.(2-1), J_r is reflected load inertia, J_t is the total inertia of system. The mechanical engineering formulas are described as the forward motion from motor input to load output.

$$\begin{cases} \dot{\theta}_l = \frac{1}{G_r}\dot{\theta}_m \\ \tau_m = \frac{1}{G_r}\tau_l \\ J_r = \frac{1}{G_r{}^2}J_l \\ J_t = J_r + J_m \end{cases} \tag{2-1}$$

According to the mechanical system, Fig. 2 is given as the block diagram of geared two–inertia

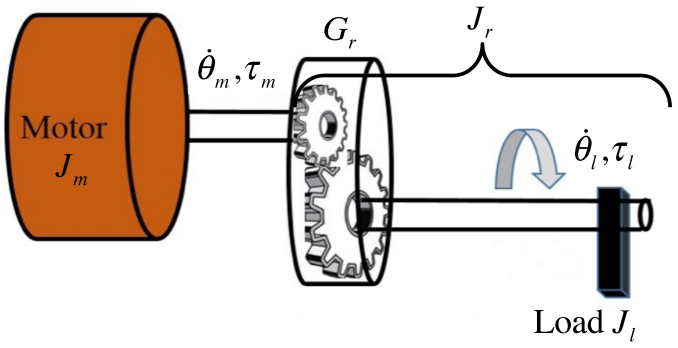

Fig. 1: The modelling of geared two–inertia system.

system. The following formulas Eq .(2-2) are the motion description of this system.

$$\begin{cases} J_m\ddot{\theta}_m = \tau_{dri} - \frac{1}{G_r}\tau_a \\ J_l\ddot{\theta}_l = \tau_a - \tau_l^{dis} \\ \tau_a = K_s(\frac{1}{G_r}\theta_m - \theta_l) \end{cases} \tag{2-2}$$

where:

J_m: exact value inertia of motor

J_l: exact value inertia of load

J_{mn}: nominal value of motor inertia

J_{ln}: nominal value of load inertia

τ_{dri}: output torque from drive motor

τ_m: torque effected on motor

K_s: the connector stiffness

θ_m: rotate angle of motor

θ_l: rotate angle of load

τ_a: torsional torque for load

τ_l^{dis}: input torque from load side

Especially the inertia of motor and load, the value of only nominal values J_{mn}, J_{ln} are used in this thesis, the difference from exact value are ignored.

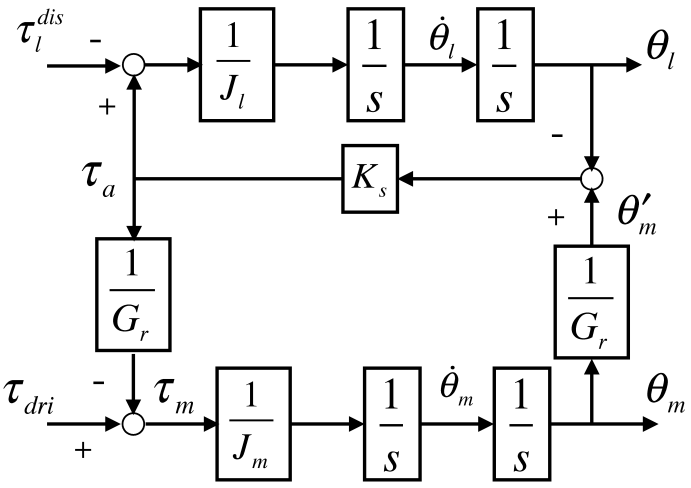

Fig. 2: Block diagram of geared two–inertia system.

From the block diagram of geared two–inertia system, the affect of gearbox through the error between decelerated motor output angle and load output angle to effect on the connection such as coupling in thesis, appearing in the torque which is output from drive motor. This motion description is also based on forward–drive of this system. In next section, the conception of forward–drive and back–drive would be clarified to lead to the discussion of back–drivability based on back–drive.

2.2.1 Motion analysis based on drive direction

In this section, the construction of motion of forward–drive and back–drive are clarified as Fig. 3. In rotational motor dynamics, torque is required to generate angular acceleration which is inversely proportional to its inertia. The physical meaning of each inertia is shown as Fig. 4.

In the situation of forward–drive, input torque is given from τ_{cmd} so that driving torque

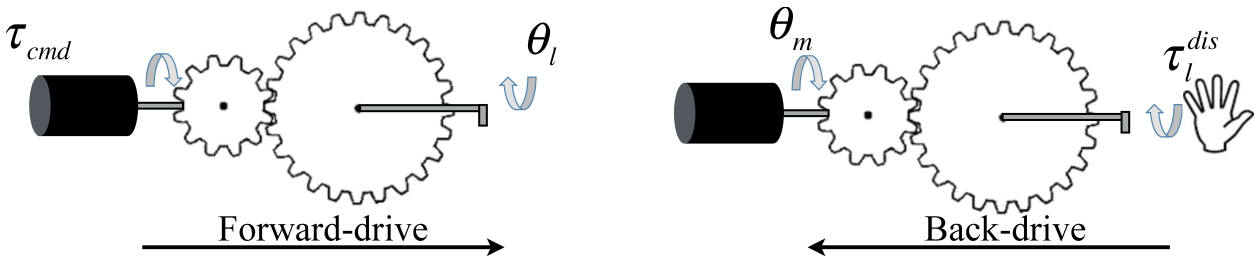

Fig. 3: Mechanical motion of forward–drive and back–drive in two–inertia system.

from motor effects on load output is followed the order from gearbox to load. In another word, driving torque from disturbance effects on load output directly firstly, acts on motor outputting through the reversed gearbox and error of angle.

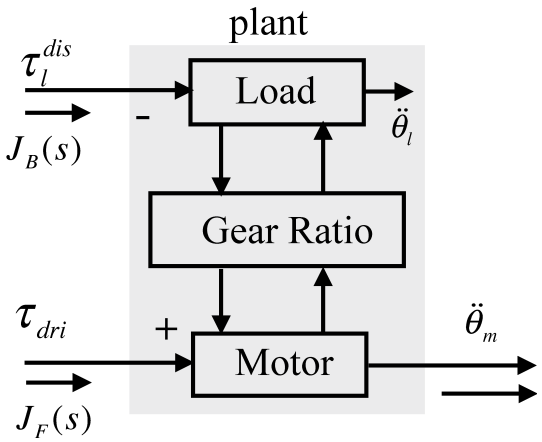

Fig. 4: Equivalent block diagram of Fig. 2

2.2.2 Drivability of forward drive based on inertia

From the left figure of Fig. 3, the motion of forward drive is a performance of driving by the command torque which is generated from motor, and outputing angle of load through gearbox. The block diagram of motion description of forward–drive is shown as Fig .5.

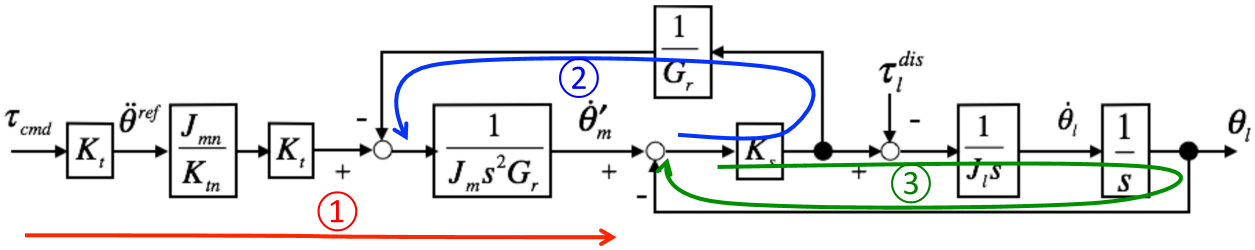

Fig. 5: Block diagram of loop order of forward–drive.

According to Fig. 4, the inertia of forward drive is described as the proportional of input torque given from driving motor and acceleration of motor. The symbol of equivalent forward–drive inertia $J_F(s)$ is brought into this system to discuss the forward motion based on geared two–inertia system. It is expressed as Eq. (2-3).

$$J_F(s) = \frac{\tau_{dri}}{\ddot{\theta}_m} = \frac{J_m G_r^2 (J_l s^2 + K_s) + J_l K_s}{G_r^2 (J_l s^2 + K_s)} = J_m + \frac{J_l K_s}{G_r^2 (J_l s^2 + K_s)} \tag{2-3}$$

In right side of Eq. (2-3), the first item J_m is the result of fraction reduction, while the second item of formula is a second order inertia element which is associated with inversely proportional of square of G_r. It is easily shown that the equivalent inertia of forward–drive includes two parts of inertia, such as motor inertia and combined inertia of load and gearbox.

The drivability is defined as an index of transmission performance from effected torque to motor acceleration. Based on this definition, the drivability is expressed as the reciprocal

expression of equivalent inertia such as Eq. (2-5).

$$G_F(s) = \frac{1}{J_F(s)} = \frac{\ddot{\theta}_m}{\tau_{tri}} \tag{2-4}$$

2.2.3 Drivability of back drive based on inertia

From the right figure of Fig. 3, the motion of back drive is expressed as a driving by the disturbed torque which is given from load side such as hand manipulation, then generating the angle of load. The rotating of motor is generated from the disturbed torque from load side through gearbox. For understanding this movement, the block diagram of motion description of back drive is shown as Fig .6. According to Fig. 5, the inertia of back drive is described as

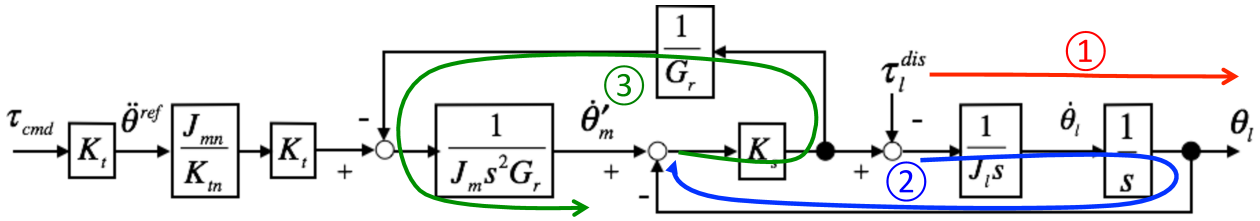

Fig. 6: Block diagram of loop order of back–drive.

the proportional of input torque given from load side and acceleration of motor. The symbol of equivalent back–drive inertia $J_B(s)$ is brought into this system to discuss the motion of back drive based on geared two–inertia system. It is expressed as Eq. (2-5).

$$J_B(s) = \frac{\tau_l^{dis}}{\ddot{\theta}_m} = -\frac{J_m G_r^2 (J_l s^2 + K_s) + J_l K_s}{K_s G_r} = -(\frac{J_m J_l G_r}{K_s} s^2 + J_m G_r + \frac{J_l}{G_r}) \tag{2-5}$$

In Eq. (2-5), the inertia of back–drive can be separated to an inversely proportional of G_r, a constant and a second order differentiation element which is associated with proportional of G_r. Based on this definition, the drivability of back drive is expressed as the reciprocal expression of equivalent inertia such as Eq. (2-6).

$$G_B(s) = \frac{1}{J_F(s)} = \frac{\ddot{\theta}_m}{\tau_l^{dis}} \tag{2-6}$$

2.3 Comparison of forward drive and back drive characteristics

In this section, the comparison of forward drive and back drive characteristics are in progress. Both bode diagrams and simulated step response are shown to describe the intuitive sensation for forward drive and back drive.

Following is the the statement of the experimental parameters shown as Tab. 1, which is used in later of this thesis.

Tab. 1: Parameters for bode diagram.

Nominal motor inertia	J_{mn}	5.8×10^{-8}	kgm^2
Nominal load inertia	J_{ln}	1.39×10^{-5}	kgm^2
Nominal torque constant	K_{tn}	0.0139	N/A
Nominal connection constant	K_{sn}	1250	
Reducer ratio	G_r	84	
Control period	T_s	0.1	ms

2.3.1 Bode diagram comparison of inertia and drivability

Based on the equations and parameters of the equivalent inertia and drivability from the previous section, the following bode diagram simulation is a shown as a comparison cases of Tab. 2.

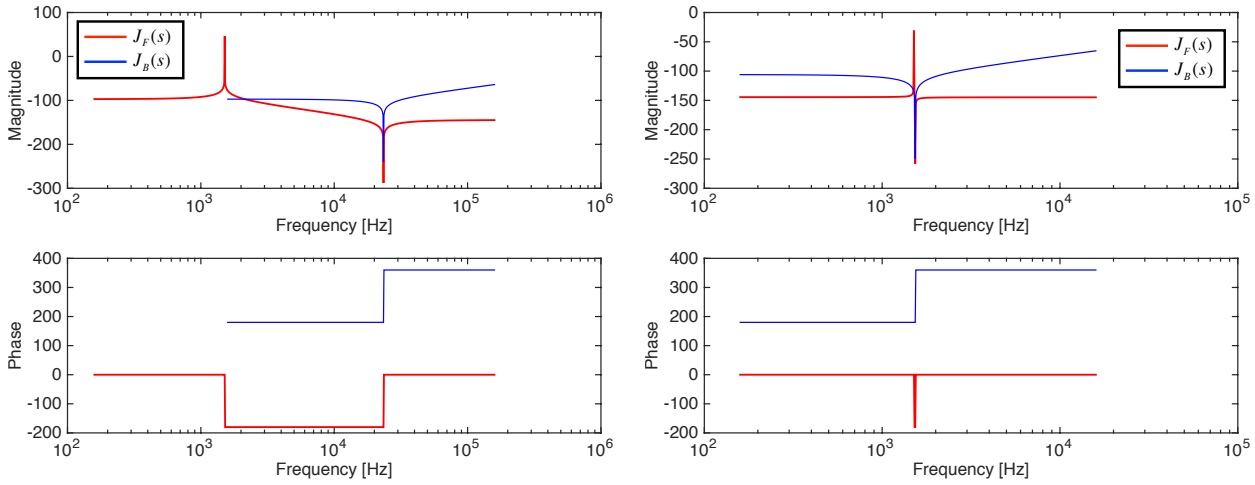

(a) Bode diagram of Sim. 1.

(b) Bode diagram of Sim. 2.

Fig. 7: Sim. 1,2: bode diagram of equivalent inertia of both directions in geared two–inertia system.

In an ordinary two–inertia system without gear ratio such as $G_r = 1$ which is shown as Fig. 7(a). According to the statement of this thesis, in the condition of without considering the damping parameter, the forward drive of proposed two–inertia system shows feature of low–pass filter with two oscillation frequencies at about 10^3 Hz and 2×10^4 Hz. The step edge of phase which is appeared so sharply explains the damping effect on frequency characteristic. There

Tab. 2: Simulation comparison of bode diagram.

Sim. 1	$J_F(s)$, $J_B(s)$	$G_r = 1$
Sim. 2	$J_F(s)$, $J_B(s)$	$G_r = 84$
Sim. 3	$G_F(s)$, $G_B(s)$	$G_r = 84$

is no magnitude difference between forward–drive inertia and back–drive inertia since no gear ratio. The bode diagram shows that forward–drive can realize the suppression in high frequency components, however, the back–drive can not be suppressed in high frequency components from the rising curve.

Fig. 7(b) is the bode diagram of forward–drive inertia and back–drive inertia according to the above two equivalent inertia formulas. It is shown that the frequency characteristic of forward–drive inertia appeared as two quite close oscillation frequencies since the gear ratio $G_r = 84$ takes apart in the calculation, which likes a full suppression controller. It is clearly seen that the magnitude difference between forward–drive inertia and back–drive inertia before the oscillation frequencies, the back–drive inertia shows more gain suppression than forward–drive inertia because of the reduce of G_r. At the same time, the back–drive still can not achieve high frequency convergence.

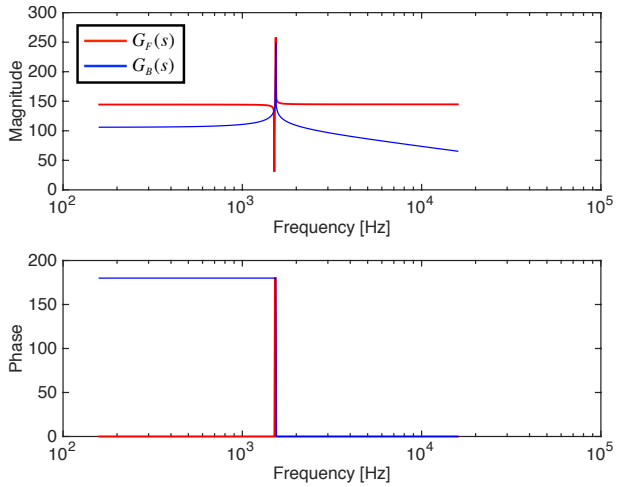

Fig. 8: Sim. 3: bode diagram of equivalent drivability of both directions in geared two–inertia system.

In Fig. 8, $G_F(s)$ is the forward–drivability based on mechanical construction without controller, while $G_B(s)$ is the back–drivability based on mechanical construction without controller. It shows the frequency characteristics opposite to those of Fig. 7(b), since the mathematical expression of drivability is the reciprocal of inertia. Under the open–loop control without regard to stability, the bode diagram of back–drivability shows a lower amplitude gain than forward–

Tab. 3: Simulation comparison of step response.

Sim. 4	Forward drive	$\tau_{tri} = 1Nm$
Sim. 5	Back drive	$\tau_l^{dis} = 1Nm$

Tab. 4: Summary of transient characteristics for mechanical control.

Mechanical control	peak time t_p	maximum overshoot M_p	convergence time t_s ($< 2\%$)
forward drive	0.0001s	3.4%	0.0042s
back drive	0.0003s	91.4%	0.0166s

drivability. So in the presence of a reducer in two–inertia system, the forward drive shows better performance in terms of both amplitude and characteristics than back drive.

2.3.2 Step responses comparison of drivability

In this thesis, the drivability can be seen as a sensitive index of torque conversion from the torque input to the motor angular acceleration output. Motion characteristics are discussed according to the expression of forward–drivability and back–drivability. The forward–drivability and back–drivability are calculated via the definition of drivability and parameters, which shown as Eq. (2-7) and Eq. (2-8).

$$G_F(s) = \frac{\ddot{\theta}_m}{\tau_{dri}} = \frac{J_l G_r^2 s^2 + K_s G_r^2}{J_m J_l G_r^2 s^2 + J_m G_r^2 K_s + J_l K_s} \tag{2-7}$$

$$G_B(s) = \frac{\ddot{\theta}_m}{\tau_l^{dis}} = -\frac{K_s G_r}{J_m J_l G_r^2 s^2 + J_m G_r^2 K_s + J_l K_s} \tag{2-8}$$

According to the calculation of ampli cation, only con- stant items are need to consider as following:

$$A_{G_F} = 20log_{10}(\frac{K_s G_r^2}{J_m G_r^2 K_s + J_l K_s}) = 20log_{10}(1.6675 \times 10^7) \tag{2-9}$$

$$A_{G_B} = 20log_{10}(|-\frac{K_s G_r}{J_m G_r^2 K_s + J_l K_s}|) = 20log_{10}(1.985 \times 10^5) \tag{2-10}$$

The following simulation case of step response based on the Tab. 3 is given to discuss the steady–state response and transient response of both forward drive and back drive.

The acceleration of motor in Fig. 9(a) and Fig. 10(a) are the forward drive and back drive of geared two–inertia system in the condition of input torque as 1 Nm, which are consistent with

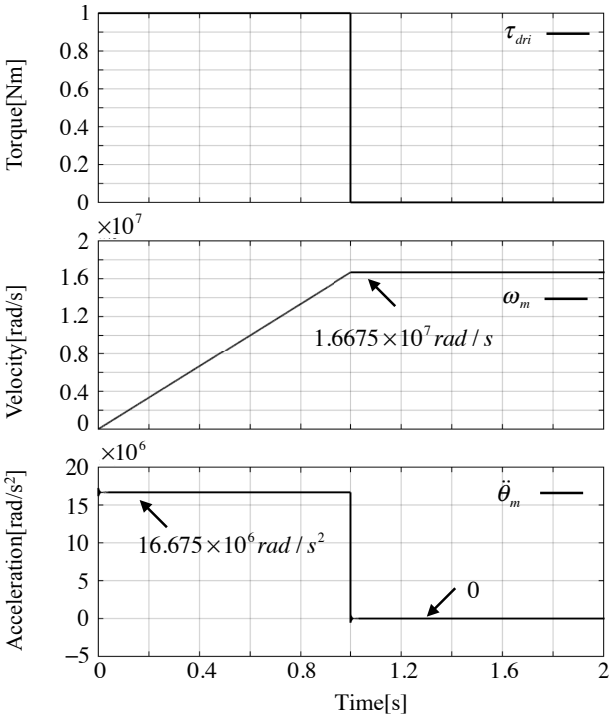

(a) review of step response.

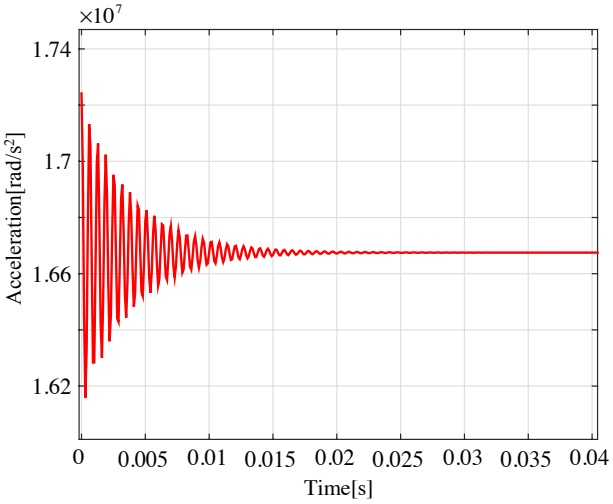

(b) transient response of acceleration.

Fig. 9: Sim. 4: step response of forward–drive in mechanical control.

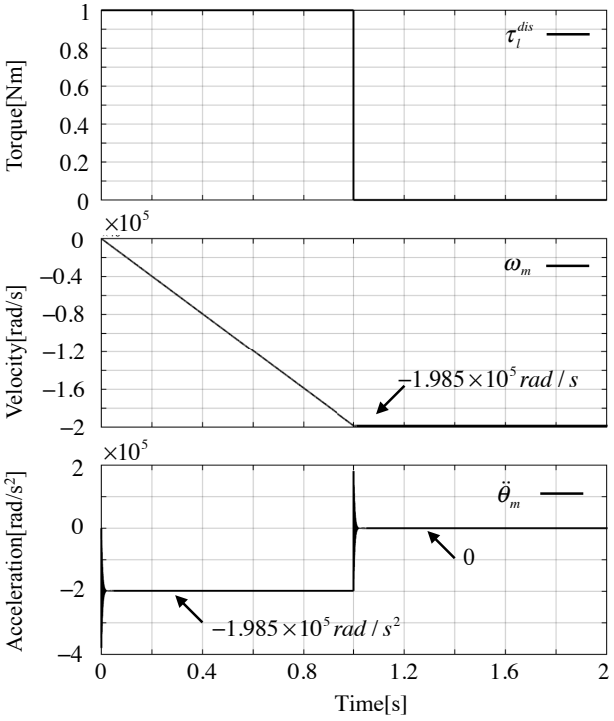

(a) review of step response.

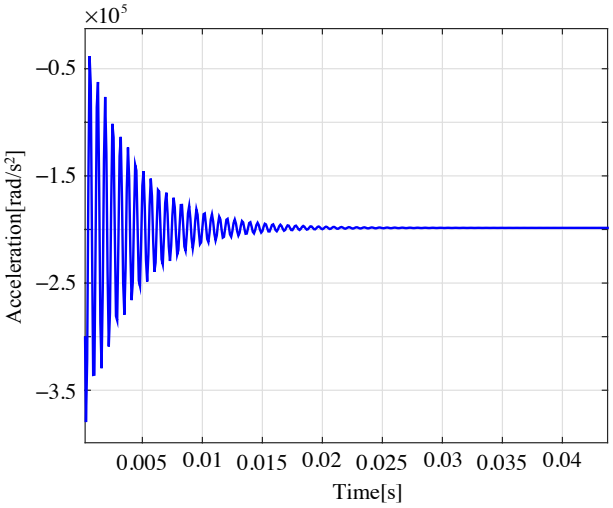

(b) transient response of acceleration .

Fig. 10: Sim. 5: step response of back–drive in mechanical control.

equation expressions. It is clearly seen that the forward–drive realizes better drivability than back–drive such as 1.6675×10^7 rad/s^2 to 1.985×10^5 rad/s^2 for the same input torque due to gear ratio.

The transient response of acceleration for both drivability are shown as Fig. 9(b) and Fig. 10(b). In the absence of consideration of damping parameters of proposed geared two–inertia system, the transient step response does not show the transient characteristics based on the mechanical structure. The time of convergence is almost the same for both forward–drivability and back–drivability.

Tab. 4 is the summary of transient response of acceleration for both drivability. Three parameters in the overshoot case were selected to present the transient characteristics under this simulation. It can be found that forward drive has better transient characteristics than back drive.

2.4 Experimental setup

According to the mechanical model used in this thesis given above, the experimental setup of geared two–inertia system is describes in detail the experimental devices, as well as the hardware equipments.

2.4.1 Overview of experimental equipment

In experiments, the equipment of geared two–inertia system is given as Fig. 11, while the mechanical parameters refer to Tab. 1. In this experiment, a Maxon DC motor (2.0 W type) with 1 : 84 gear ratio is selected as the drive motor. The inertial load which consists of another Maxon DC motor (150 W type), is connected to the drive motor by a coupling.

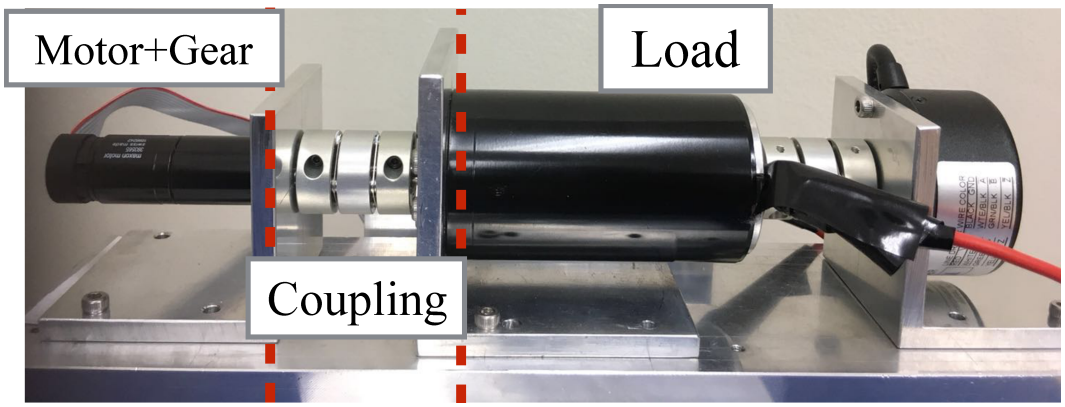

Fig. 11: The equipment of geared two–inertia system used in experiments.

2.4.2 Supporting equipments

Fig. 12 is the driver module for drive motor. It is also the Maxon company's product.

Model /Items	ESCON 36/2
Output current (nominal)	2.0 A
Output current (maximum)	4.0 A

Fig. 12: The driver for drive motor.

In order to give a stable external torque for achieving back drive, a load motor with an output torque, which is driving by Fig. 13 shown driver module, is used to mount the load part of the drive motor. It is a general servo motor driver product of Co. ServoTechno.

Model /Items	PMA6
Output current (nominal)	6.0 A
Output current (maximum)	15.0 A

Fig. 13: The driver for load motor.

Two angle encoders are implemented to both motor and load side with the resolution proportion following the gear reduction. The angle encoder of drive motor that assembled directly on the motor is 512 plus/r. Due to the presence of the reducer as $G_r = 84$, the resolution of angle encoder for load motor is needed to be at least 84 times the one of drive motor. Fig. 14 is the encoder for load motor, which is the product of Co. MicroTech Laboratory, with the resolution of $8192 \times 8 = 65536$ plus/r. Via this design, the external torque input could be emulated with torque output of load motor as well as drive motor.

As a result, later in this thesis the simulations and experiments are all based on the model parameters above.

Model /Items	MES-30-819 2PST8E
Multiplication circuit	8
Output plus	8192 p/r
Allowable maximum speed (mechanical)	6000r/min

Fig. 14: The encoder for load motor.

2.5 Summary of this chapter

From the discussion in this chapter, it is clearly that according to increasing of gear ratio, $J_F(s)$ gets much smaller than $J_B(s)$, so that the back–drive become much difficult to realise than forward–drive due to gear ratio and friction.

Based on this perception of drivability, a designed controller is considered in view of torque control conversion from back–drive to forward drive. The description of back–drivability is designed based on a referenced forward–drivability to evaluate the performance of control strategy.

Chapter 3

Conventional Method and Control Components

3.1 Introduction

Before presenting the proposed control strategy, the controller elements used in this thesis and a conventional torque control [21] for back–drive is introduced as a contrast in this chapter. This control method uses the most concise control components for torque control. In this chapter, the characteristics of these components, which are based on the conventional method but are also used in later proposed method, are also described in detail.

3.2 Conventional control method

The conventional torque control with torque gain C_t is shown as Fig. 15. It shows a load–side torque control system based on motor–side acceleration control including the dynamics of DOB. In that paper, the bidirectional drivability matrix of the load–side torque control is derived as follow, even if both forward–drive and back–drive drivability are described from input torque to output velocity, which is different from the definition of this thesis.

$$\begin{bmatrix} \omega_m \\ \omega_l \end{bmatrix} = \begin{bmatrix} G_{fb}(s) & G_b(s) \\ G_f(s) & G_{bf}(s) \end{bmatrix} \begin{bmatrix} \tau_{cmd} \\ \tau_l^{dis} \end{bmatrix} \tag{3-1}$$

The conventional control method are based on the disturbance observer and load–side disturbance observer, which are also the control elements utilized in this thesis.

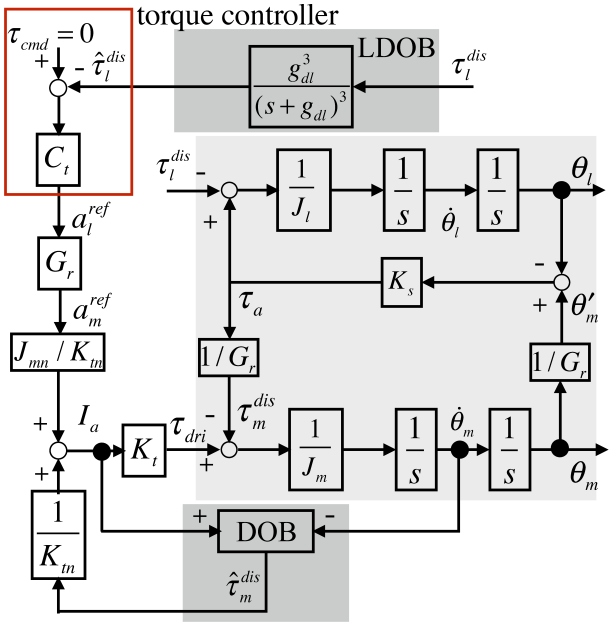

Fig. 15: Conventional load–side torque control based on DOB and LDOB.

3.3 Disturbance observer

In general, disturbance observer introduces an acceleration controller to estimate and cancel the disturbance torque as quickly as possible. The estimated disturbance torque is obtained from the motor velocity $\dot{\theta_m}$ and current reference I^{ref} shown in the red frame of Fig. 19. The disturbance torque τ_m^{dis} is denoted as Eq. 3-2 and Eq. 3-3.

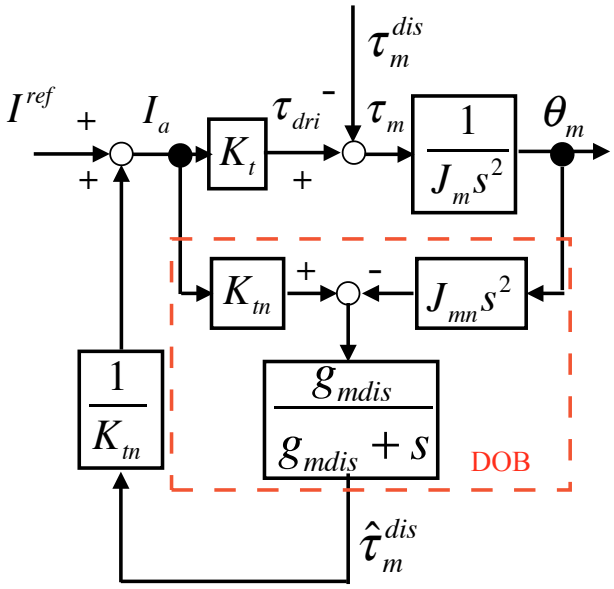

Fig. 16: Block diagram of disturbance observer.

$$\tau_m^{dis} = (J_m - J_{mn})\ddot{\theta}_m + (K_{tn} - K_t)I^{ref} + \tau_{fric} + \tau_{reac} \tag{3-2}$$

$$\hat{\tau}_m^{dis} = \frac{g_{mdis}}{s + g_{mdis}} \tau_m^{dis} \tag{3-3}$$

Where,

τ_{fric}: coulomb friction

τ_{reac}: torsional reaction torque to motor

$$K_t = K_{tn}, J_m = J_{mn}, J_l = J_{ln} \tag{3-4}$$

From above construction of DOB, the difference between nominal value and exact value in first and second term are compensated by $\hat{\tau}_m^{dis}$ which is given through a low–pass filter with cut–off frequency g_{mdis} in Eq. (3-3). Reaction force observer (RFOB) [32] is also a useful tool to estimate reaction force by eliminating friction force τ_{fric} without force sensor. In this research, a RFOB just simply estimates all disturbance torques without consideration of friction model. In other words, not only friction but also reaction disturbance are as feedback from RFOB to input. Therefore, as Eq. (3-4), the nominal value of inertia of motor, load and torque constant (J_{mn}, J_{ln}, K_{tn}) are used in this paper to replace identification of the exact value of them. In the calculation of the rest of this paper, the difference between exact value and nominal value would be ignored to simplify the representation.

3.4 Friction compensation based on DOB

One of the important reasons to make the back–drivability of geared two–inertia system deteriorate is the influence of friction as Eq. 3-2. Especially, the fiction components include twi items as Eq. (3-5)

$$\tau_{ric} = \tau_c + D_e\dot{\theta} \tag{3-5}$$

where:

τ_c: Coulomb friction

D_e: Viscous friction constant

$\dot{\theta}$: Velocity of motion

A lot of researchers prefer to identify the exact friction modelling parameter D_e and coulomb friction curve via torque sensor. In this thesis, the friction of system is compensated in the condition without exactly correct friction model [31] for the sake of disturbance observer. Since the DOB is able to reject disturbances, it increases the motor impedance significantly [20]. It brings to good effect to forward–drive because the compensated torque is contributed to drive side of motor to generate more torque. However, in back–drive, the fed back torsional reaction torque τ_{reac} is performed as the motor impedance to reduce the velocity of motor output

instead. In other words, it is a tradeoff between dynamic properties and friction compensation while keeping off the complicated calculation. At the same time, a way of remedy is employed by selecting a lower cut–off frequency of DOB in this paper to reduce the high frequency components of estimated torsional reaction torque. Fig. 17 shown the compensation principle.

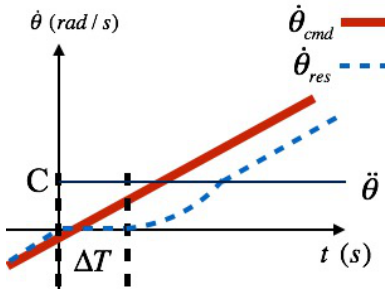

Fig. 17: Velocity response w/o disturbance observer by velocity control in forward–driving.

In a pure velocity control with a given constant acceleration, the command velocity is shown as the red sold line. The influence of coulomb friction is appeared in the period of zero velocity. After δt, the drive torque is increased to overcome the the friction to realising velocity tracking. Blue dotted line shows this phenomenon.

Experimental result to verily the effectiveness is shown as Fig. 18. From this figure, purple

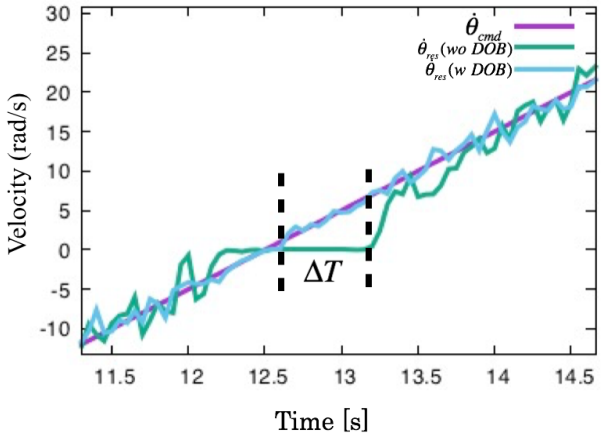

Fig. 18: Velocity response of motor w and w/o disturbance observer in forward–driving.

sold line is the command velocity. Light blue sold line shows the velocity response with the compensation of disturbance observer, while the green sold line shows the velocity response without disturbance observer. The effectiveness of compensation of friction could be clearly seen. In physically, the disturbance observer compensates in advance the stored torque to drive side. Since the back–driving is conversed to forward–driving via the strategy 1, in the condition of the back–driving motion. the friction compensation also achieved.

3.5 Load–side disturbance observer

In order to design a proposed back–drivability, a load–side disturbance observe is needed to implement for estimating the external torque to achieve torque control. In this subsection, a similar structure of DOB is used for load–side disturbance observer shown as Eq. (3-6).

$$\hat{\tau}_l^{dis} = \frac{g_{ldis}}{s + g_{ldis}}((K_s - K_{sn})(\theta_l - \frac{1}{G_r}\theta_m) + (J_l - J_{ln})s\dot{\theta}_l + \tau_l^{dis}) \tag{3-6}$$

Fig. 15 is the block diagram of motion control based on load–side disturbance observer. From this figure, load–side disturbance observer calculates the disturbance torque of load τ_l^{dis} from difference between the nominal torsional torque and nominal load–inertia torque. In this thesis, estimated velocity response pseudo–differentially comes from the rotate angle encoder, which also achieve the acceleration control of disturbance observer by second order pseudo–differentiation. It is estimated though a low–pass filter with cut–off frequency of g_{ldis}, so that feedback to motor side.

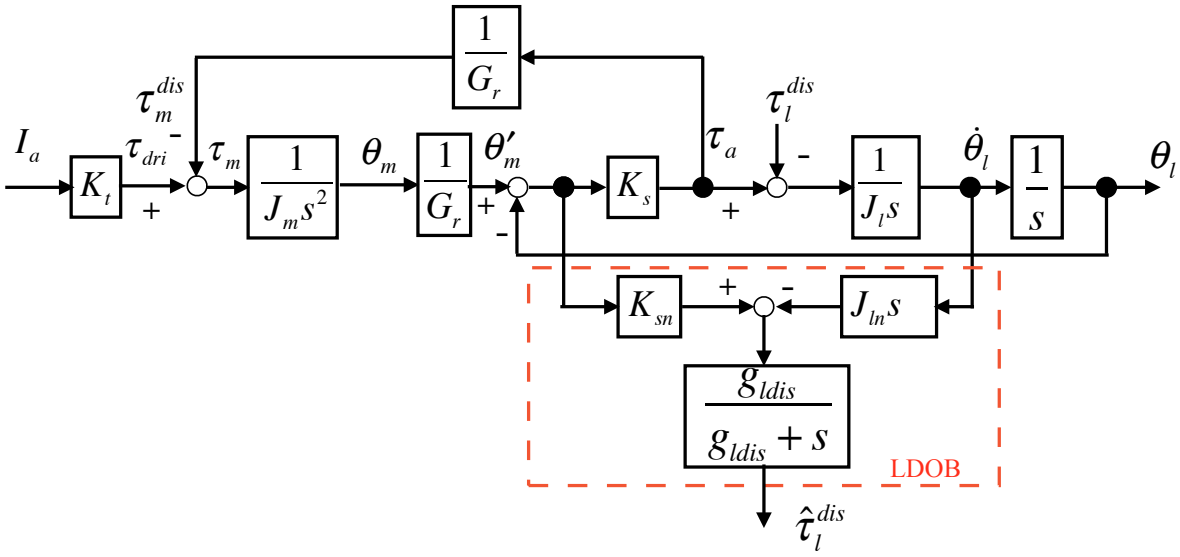

Fig. 19: Bode diagram of load–side disturbance observer.

3.6 Summary

Considering the robustness of system, DOB is one of the widely recognized robust motion control compared with complicated sliding control and fuzzy control. However, DOB brings an estimation delay to system but a high–performance DOB is not intended for geared two–inertia system [31]. Even though the motion control with DOB could not achieve high robustness

against a step torque input from load–side, it still worth to use DOB to reduce the calculation of constructing the characteristic of back–drivability in proposed method.

In following, the progressing of consideration to design the proposed back–drivability is discussed.

Chapter 4

Strategy of Torque Control for Improving Back–drivability

4.1 Introduction

In this chapter, the mathematic expression of performance of back–drivability is shown to evaluate progressive control results with step–by–step controllers. A proposed semi–closed loop of torque control based on Disturbance Observe (DOB) and Load–side Disturbance Observer (LDOB) are implemented to geared two–inertia system to improve the back–drivability by three steps. A feedback controller is designed based on the target of estimation of forward–drive, in addition, the scaling α is also introduced to designed controller to make the performance of back–drivability adjustable.

4.2 Step 1: Constructing a reference equivalent inertia

According to the discussion of previous chapter, the forward–drive inertia of geared two–inertia system achieve higher transparency from torque input to rotating acceleration than through the back–drive inertia both in mathematic expression and bode diagram verification, especially in the condition of increasing of gear ratio G_r. As Fig. 20 shows, In first step, back–driving as a motion control which is equivalently defined with back–drive inertia in this thesis, is considered to converse to forward–drive to achieve higher performance of itself. The back–drivability, the performance of back–driving, also can be evaluated by the performance of conversed forward–drive control results.

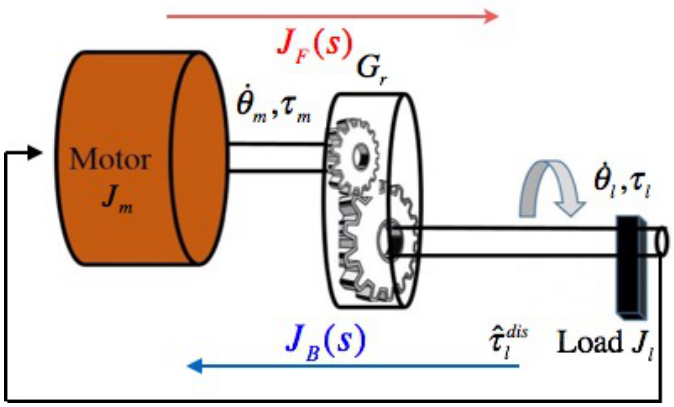

Fig. 20: Schematic diagram of conversion of control inertial based on geared two–inertia system.

4.2.1 Drivability of referenced forward drive control

In the previous introduction, the drivability of forward drive is considered in pure mechanical motion of open–loop, so that the definition of drivability is referred as following Eq. (4-1):

$$G_{FD}(s) = \frac{\ddot{\theta}_m}{\tau_{dri}} = \frac{G_r^2(J_l s^2 + K_s)}{J_m G_r^2(J_l s^2 + K_s) + J_l K_s} = G_F(s) \tag{4-1}$$

From the control system of Fig. 21, which neglects the effect of friction, it is shown that, if we consider as the effected torque and only describe the expression of plant of motor, the expression of back–drivability is same with open loop of mechanical forward–drive. However, the effect of parameters such as force gain and cut–off frequency could not clarified in this equation. Therefore, taking τ_{cmd} into the expression shown as Eq. (4-2).

$$\tau_{dri} = \tau_{cmd} K_f J_m + (1 - K_f J_m) \frac{J_l K_s g_{mdis}}{G_r^2(J_l s^2 + K_s)(s + g_{mdis})} \ddot{\theta}_m \tag{4-2}$$

As a result, the new forward–drivability is given for showing the transmission performance from command torque to output motor acceleration. $G'_{FD}(s)$ is shown as Eq. (4-3).

$$\begin{aligned} G'_{FD}(s) &= \frac{\ddot{\theta}_m}{\tau_{cmd}} \\ &= \frac{K_f J_m G_r^2(J_l s^2 + K_s)(s + g_{mdis})}{J_m G_r^2(J_l s^2 + K_s)(s + g_{mdis}) + J_l K_s s + K_f J_m J_l K_s g_{mdis}} \\ &= \frac{b_{FD3} s^3 + b_{FD2} s^2 + b_{FD1} s + b_{FD0}}{a_{FD3} s^3 + a_{FD2} s^2 + a_{FD1} s + a_{FD0}} \end{aligned} \tag{4-3}$$

$$b_{FD3} = K_f J_m G_r^2 J_l,$$
$$b_{FD2} = K_f J_m G_r^2 J_l g_{mdis},$$
$$b_{FD1} = K_f J_m G_r^2 K_s,$$
$$b_{FD0} = K_f J_m G_r^2 K_s g_{mdis},$$
$$a_{FD3} = J_m G_r^2 J_l,$$
$$a_{FD2} = J_m G_r^2 J_l g_{mdis},$$
$$a_{FD1} = K_s (J_m G_r^2 + J_l),$$
$$a_{FD0} = J_m K_s g_{mdis} (G_r^2 + K_f J_l)$$

From now on, this new functional relationship of forward–drivability is used in this thesis for

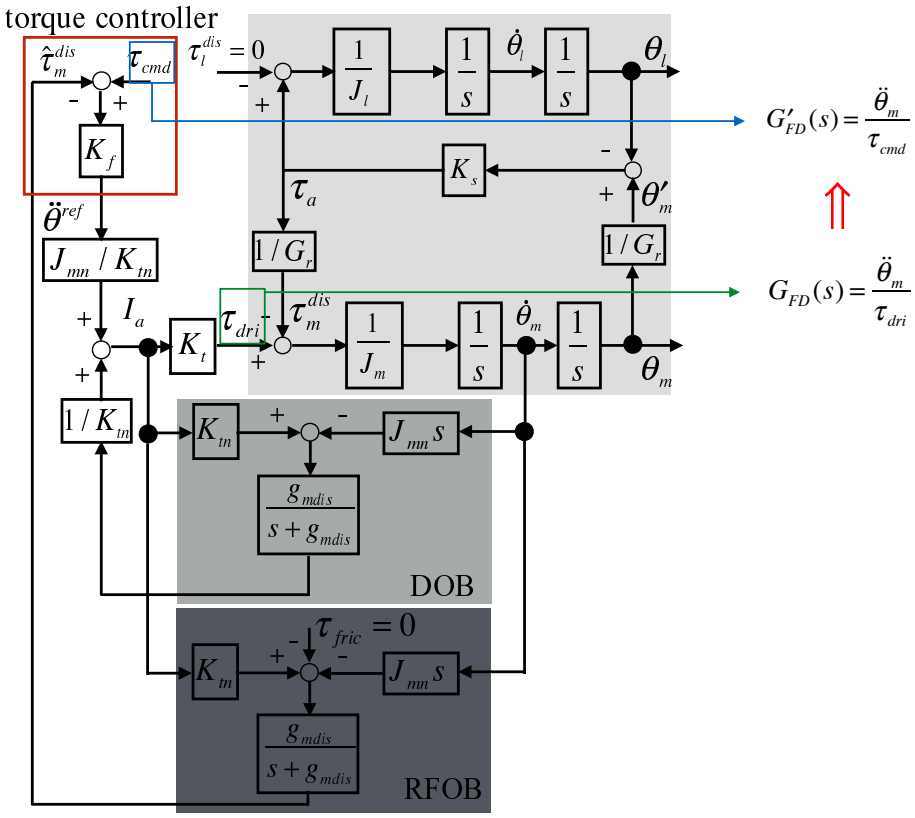

Fig. 21: Block diagram of forward–drive feedback control with DOB.

later comparison with conventional method and various evaluation analysis. In Eq. (4-3) of forward–drivability, we can find that it is a high–order dynamic representation.

4.2.2 Drivability of designed back drive control based on reference equivalent inertia

First, constructing the proposed back drive as Fig. 22. Calculating the expression of back–drivability of Fig. 22 and the minus sign is the direction of input signal. It is shown as Eq. (4-5).

$$G_{BD}(s) = -\frac{H(s)J_m G_r^2(J_l s^2 + K_s)(s + g_{mdis})\frac{g_{ldis}}{s+g_{ldis}} + G_r K_s s}{J_m G_r^2(J_l s^2 + K_s)(s + g_{mdis}) + J_l K_s s}$$
$$= -\frac{b_{BD3}s^3 + b_{BD2}s^2 + b_{BD1}s + b_{BD0}}{a_{BD4}s^4 + a_{BD3}s^3 + a_{BD2}s^2 + a_{BD1}s + a_{BD0}} \quad (4\text{-}4)$$

$$b_{BD3} = H(s)J_m G_r^2 J_l g_{ldis},$$
$$b_{BD2} = H(s)J_m G_r^2 J_l g_{mdis} g_{ldis},$$
$$b_{BD1} = G_r K_s g_{ldis}(H(s)J_m G_r + 1),$$
$$b_{BD0} = H(s)J_m G_r^2 K_s g_{mdis} g_{ldis},$$
$$a_{BD4} = J_m G_r^2 J_l,$$
$$a_{BD3} = J_m G_r^2 J_l(g_{mdis} + g_{ldis}),$$
$$a_{BD2} = J_m G_r^2(J_l g_{mdis} g_{ldis} + K_s),$$
$$a_{BD1} = J_m G_r^2 K_s(g_{mdis} + g_{ldis}) + J_l K_s g_{ldis},$$
$$a_{BD0} = J_m G_r^2 K_s g_{mdis} g_{ldis}$$

In next step, the strategy of constructing back–drivability based on referenced forward–drivability is discussed.

4.3 Step 2: Constructing controller $H(s)$ for back–drivability

In this section, a semi-closed loop torque control of geared two–inertia system based on load–side disturbance observer is implemented to discuss the improvement of back–drivability. The constructing the proposed back-drivability to consistent with referenced forward–drivability. A scaling factor α is introduced to realize adjusted drivability such as Eq. (4-5).

$$G_{BD}(s) = -\alpha\ G'_{FD}(s)\ (\alpha > 0) \quad (4\text{-}5)$$

Bringing Eq. (4-3) and Eq. (4-5) into Eq. (4-5) as Eq. (4-6).

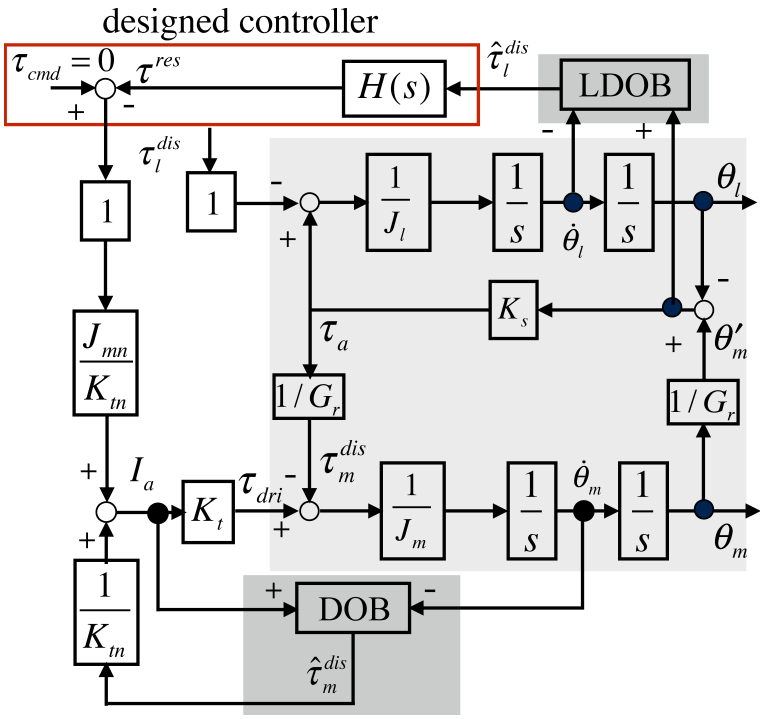

Fig. 22: Block diagram of designed back–drive control based on DOB and LDOB.

$$\frac{b_{BD3}s^3+b_{BD2}s^2+b_{BD1}s+b_{BD0}}{a_{BD4}s^4+a_{BD3}s^3+a_{BD2}s^2+a_{BD1}s+a_{BD0}} = -\alpha\frac{b_{FD3}s^3+b_{FD2}s^2+b_{FD1}s+b_{FD0}}{a_{FD3}s^3+a_{FD2}s^2+a_{FD1}s+a_{FD0}}\ (\alpha>0) \tag{4-6}$$

Before solving this equation to get the expression of $H(s)$, it is easy to find that the order of numerator in back–drivability is not consistent with the order of forward–drivability. So, a low–pass filter is implemented to the control of forward–drive that is defined as $G_{FDL}(s)$ to achieve the same dynamic characteristic as Eq. (4-7).

$$G_{FDL}(s)=\frac{g_{LPF}}{s+g_{LPF}}G'_{FD}(s) \tag{4-7}$$

And then the design strategy is rewritten as Eq. (4-8).

$$G_{BD}(s)=-\alpha G_{FDL}(s)\ (\alpha>0) \tag{4-8}$$

Expanding Eq. (4-8), Eq. (4-9) is the complete expression of constructing proposed back–drivability.

$$
\begin{aligned}
&\frac{b_{BD3}s^3 + b_{BD2}s^2 + b_{BD1}s + b_{BD0}}{a_{BD4}s^4 + a_{BD3}s^3 + a_{BD2}s^2 + a_{BD1}s + a_{BD0}} \\
&= -\alpha \frac{g_{LPF}}{s + g_{LPF}} \frac{b_{FD3}s^3 + b_{FD2}s^2 + b_{FD1}s + b_{FD0}}{a_{FD3}s^3 + a_{FD2}s^2 + a_{FD1}s + a_{FD0}} \\
&= -\alpha \frac{b_{FDL3}s^3 + b_{FDL2}s^2 + \cdots + b_{FDL0}}{a_{FDL4}s^4 + a_{FDL3}s^3 + \cdots + a_{FDL0}} \ (\alpha > 0)
\end{aligned} \tag{4-9}
$$

$$
\begin{aligned}
b_{FDL3} &= g_{LPF} b_{FD3}, \\
b_{FDL2} &= g_{LPF} b_{FD2}, \\
b_{FDL1} &= g_{LPF} b_{FD1}, \\
b_{FDL0} &= g_{LPF} b_{FD0}, \\
a_{FDL4} &= a_{FD3}, \\
a_{FDL3} &= a_{FD2} + g_{LPF} a_{FD3}, \\
a_{FDL2} &= a_{FD1} + g_{LPF} a_{FD2}, \\
a_{FDL1} &= a_{FD0} + g_{LPF} a_{FD1}, \\
a_{FDL0} &= g_{LPF} a_{FD0}
\end{aligned}
$$

Therefore, the solution of expression $H(s)$ is shown as Eq. (4-10). By the way, for simplifying the calculation, we let the cut–off frequency of LDOB (g_{ldis}) to be consistent to low–pass filter g_{LPF} in this paper.

$$
\begin{aligned}
H(s) &= \alpha K_f \frac{J_m G_r^2 (J_l s^2 + K_s)(s + g_{mdis}) + J_l K_s s}{J_m G_r^2 (J_l s^2 + K_s)(s + g_{mdis}) + J_l K_s s + K_f J_m J_l K_s g_{mdis}} \\
&- \frac{K_s s (s + g_{ldis})}{J_m G_r g_{ldis} (J_l s^2 + K_s)(s + g_{mdis}) g_{ldis}} \\
&= \frac{b_{H6}s^6 + b_{H5}s^5 + b_{H4}s^4 + b_{H3}s^3 + b_{H2}s^2 + b_{H1}s + b_{H0}}{a_{H6}s^6 + a_{H5}s^5 + a_{H4}s^4 + a_{H3}s^3 + a_{H2}s^2 + a_{H1}s + a_{H0}}
\end{aligned} \tag{4-10}
$$

Of these, each items are expanded as follows:

$$
\begin{aligned}
b_{H6} &= \alpha K_f J_m^2 G_r^4 J_l^2 g_{LPF}, \\
b_{H5} &= 2\alpha K_f J_m^2 G_r^4 J_l^2 g_{mdis} g_{LPF} - J_m G_r^3 J_l K_s, \\
b_{H4} &= \alpha K_f J_m G_r^2 J_l g_{LPF} (J_m G_r^2 J_l g_{mdis}^2 + 2 J_m G_r^2 K_s + J_l K_s) - J_m G_r^3 J_l K_s (g_{mdis} + g_{ldis}), \\
b_{H3} &= J_m G_r^2 J_l K_s g_{mdis} g_{LPF} (4\alpha K_f J_m G_r^2 + \alpha K_f J_l - G_r) - G_r K_s^2 (J_l + J_m G_r^2), \\
b_{H2} &= \alpha K_f J_m^2 G_r^4 K_s (2 J_l g_{mdis}^2 g_{LPF} + K_s g_{LPF}) - G_r J_l K_s^2 g_{ldis} \\
&\quad + K_f J_m G_r J_l K_s^2 (\alpha G_r g_{LPF} - g_{mdis}) - J_m G_r^3 K_s^2 (g_{mdis} + g_{ldis}), \\
b_{H1} &= \alpha K_f J_m G_r^2 K_s^2 g_{mdis} g_{LPF} (J_l + 2 J_m G_r^2) - J_m G_r K_s^2 g_{mdis} g_{ldis} (K_f J_l + G_r^2), \\
b_{H0} &= \alpha K_f J_m^2 G_r^4 K_s^2 g_{mdis}^2 g_{LPF},
\end{aligned}
$$

$$
\begin{aligned}
a_{H6} &= J_m^2 G_r^4 J_l^2 g_{ldis}, \\
a_{H5} &= 2J_m^2 G_r^4 J_l^2 g_{mdis} g_{ldis}, \\
a_{H4} &= J_m G_r^2 J_l g_{ldis} (J_m G_r^2 J_l g_{mdis}^2 + 2J_m G_r^2 K_s + J_l K_s), \\
a_{H3} &= J_m G_r^2 J_l K_s g_{mdis} g_{ldis} (K_f J_m J_l + 4J_m G_r^2 + J_l), \\
a_{H2} &= J_m^2 G_r^2 J_l K_s g_{mdis}^2 g_{ldis} (K_f J_l + 2G_r^2) + J_m G_r^2 K_s^2 g_{ldis} (J_m G_r^2 + J_l), \\
a_{H1} &= J_m G_r^2 K_s^2 g_{mdis} g_{ldis} (K_f J_m J_l + 2J_m G_r^2 + J_l), \\
a_{H0} &= J_m^2 G_r^2 K_s^2 g_{mdis}^2 g_{ldis} (G_r^2 + K_f J_l)
\end{aligned}
$$

4.4 Step 3: The back–drivability based on reference forward–drivability

Finally, the expanded expression of back–drivability $G_{BDH}(s)$ is shown as Eq. (4-11) by introducing Eq. (4-10),

$$
G_{BDH}(s) = -\alpha \frac{(b_{BDH9} s^9 + \cdots + b_{BDH4} s^4) + \cdots + b_{BDH0}}{(a_{BDH10} s^{10} + \cdots + a_{BDH5} s^5) + \cdots + a_{BDH0}} \tag{4-11}
$$

$$
\begin{aligned}
b_{BDH0} &= \alpha K_f J_m G_r^2 K_s g_{mdis} g_{LPF} = b_{FDL0}, \\
a_{BDH0} &= J_m K_s g_{mdis} g_{LPF} (G_r^2 + K_f J_l) = a_{FDL0}
\end{aligned}
$$

The 10–orders polynomial coefficients of transfer function $G_{BDH}(s)$ is the expanded form as Eq. (4-5). The higher components in brackets are suppose to be zero. According to the constant items, the amplification of referenced forward–drivability is as follow:

$$
\begin{aligned}
&A_{G_{FDL}} = 20log_{10}(\frac{b_{FDL0}}{a_{FDL0}}) \\
&= 20log_{10}(\frac{\alpha K_f}{1 + 1.97^{-9} K_f}) \\
&\doteq 20log_{10}(\alpha K_f) \\
&= A_{G_{BDH}}
\end{aligned} \tag{4-12}
$$

According to the small value of K_f, the item $1.97^{-9} K_f \leq 1$, so that the amplification of referenced forward–drivability is only in proportion to torque gain K_f and scaling factor α.

Here, let's review the constant items of continuous expression of controller $H(s)$:

$$
\begin{aligned}
&b_{H0} = \alpha K_f J_m^2 G_r^4 K_s^2 g_{mdis}^2 g_{LPF}, \\
&a_{H0} = J_m^2 G_r^2 K_s^2 g_{mdis}^2 g_{ldis} (G_r^2 + K_f J_l) \\
&A_{G_H} = 20log_{10}(\frac{b_{H0}}{a_{H0}}) \\
&= 20log_{10}(\frac{\alpha K_f}{1 + 1.97^{-9} K_f}) \\
&\doteq 20log_{10}(\alpha K_f)
\end{aligned}
\tag{4-13}
$$

It is shown that Eq. (4-13) is same with the Eq. (4-12), which means the designed back–drivability contributes from the controller $H(s)$ entirely.

4.5 Summary of this chapter

In this chapter, as Fig. 23 is the proposed block diagram of torque control with DOB, LDOB and the designed controller, the design strategy of proposed scaled back–drivability torque control based on disturbance observer and load–side disturbance observe is discussed. The method is considered in the view of conversion of drive inertia which comes from the thinking of difference from forward–drive inertia and back–drive inertia. The strategy of constructing the proposed back–drivability to consistent with referenced forward–drivability by calculating the controller $H(s)$.

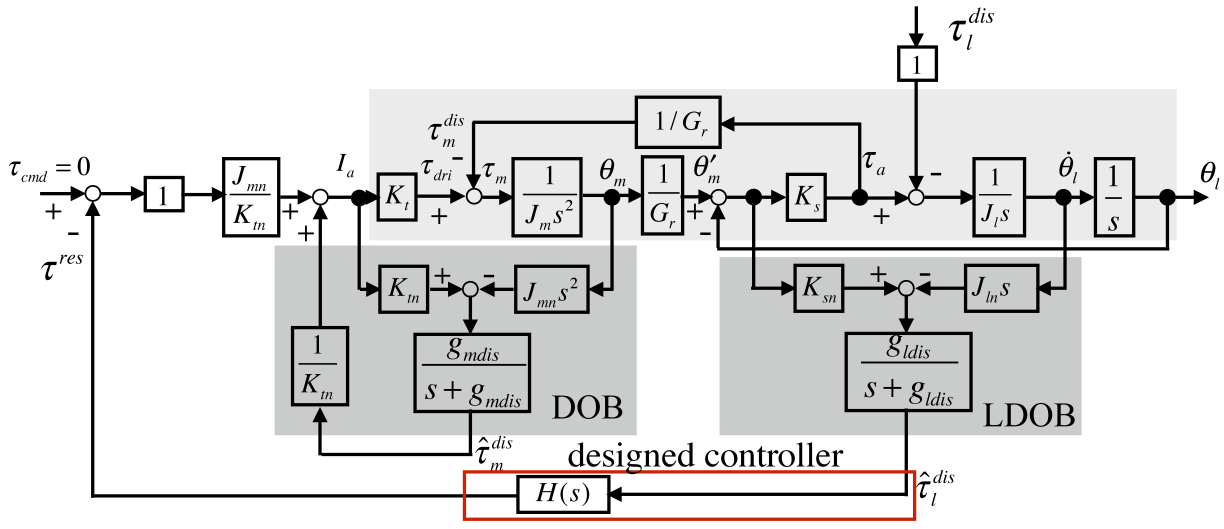

Fig. 23: Block diagram of proposed back–drive with designed controller.

Chapter 5

Parameters Discussion

5.1 Introduction

In previous two chapters, the proposed back–drive control are discussed in detail. In order to construct $H(s)$, many design parameters other than mechanical ones are introduced, such as g_{mdis}, g_{ldis}, g_{LPF}. The selection of these parameters can affect the stability and performance of the system. In this chapter,the stability statement and parameters discussion are in progress.

5.2 Parameters design

In this thesis, there are three different cut–off frequencies implemented in controller for DOB, LDOB and low–pass filter, respectively. However, even if there is no physical meaning to discuss the stability in this thesis, the three parameters of cut–off frequency matter the stability and robustness of the proposed system. The design methods of cut–off frequency based on the root locus of back–drivability are explained one by one in this section.

5.2.1 Cut–off frequency of DOB

First, the compensation of DOB is discussed at first. It is easy to observe the cut–off frequency of DOB affects the location of poles of Eq. (5-1). By bringing in the expression of $H(s)$ described before, the transfer function $G_{BD}(s)$ is a expression with denominator of 11 orders and a numerator of 10 orders.

$$\begin{aligned} G_{BD}(s) &= -\frac{H(s)J_m G_r^2(J_l s^2 + K_s)(s + g_{mdis})\frac{g_{ldis}}{s+g_{ldis}} + G_r K_s s}{J_m G_r^2(J_l s^2 + K_s)(s + g_{mdis}) + J_l K_s s} \\ &= -\frac{b_{BD3}s^3 + b_{BD2}s^2 + b_{BD1}s + b_{BD0}}{a_{BD4}s^4 + a_{BD3}s^3 + a_{BD2}s^2 + a_{BD1}s + a_{BD0}} \end{aligned} \tag{5-1}$$

Without the cancellation of zero-pole of $G_{BD}(s)$, the poles and zeros in the condition of $Kf = 1724$ are shown as follow.

Tab. 5: Zero-poles in different g_{mdis}.

poles and zeros	$g_{mdis} = 100$	$g_{mdis} = 500$	$g_{mdis} = 1000$
$p_1 = 10^3\times$	$-0.0016 + 9.6427i$	$-0.0082 + 9.6423i$	$-0.0163 + 9.6411i$
$p_2 = 10^3\times$	$-0.0016 - 9.6427i$	$-0.0082 - 9.6423i$	$-0.0163 - 9.6411i$
$p_3 = 10^3\times$	$-0.0016 + 9.6427i$	$-0.0082 + 9.6423i$	$-0.0163 + 9.6411i$
$p_4 = 10^3\times$	$-0.0016 - 9.6427i$	$-0.0082 - 9.6423i$	$-0.0163 - 9.6411i$
$p_5 = 10^3\times$	$0.0000 + 9.4830i$	$-0.0000 + 9.4830i$	$0.0000 + 9.4830i$
$p_6 = 10^3\times$	$0.0000 - 9.4830i$	$-0.0000 - 9.4830i$	$0.0000 - 9.4830i$
$p_7 = 10^3\times$	$-1.0000 + 0.0000i$	$-1.0000 + 0.0000i$	$-1.0001 + 0.0001i$
$p_8 = 10^3\times$	$-1.0000 + 0.0000i$	$-1.0000 - 0.0000i$	$-1.0001 - 0.0001i$
$p_9 = 10^3\times$	$-0.1000 + 0.0000i$	$-0.5000 + 0.0000i$	$-0.9999 + 0.0000i$
$p_{10} = 10^3\times$	$-0.0967 + 0.0000i$	$-0.4836 + 0.0000i$	$-0.9675 + 0.0000i$
$p_{11} = 10^3\times$	$-0.0967 + 0.0000i$	$-0.4836 + 0.0000i$	$-0.9675 + 0.0000i$
$z_1 = 10^3\times$	$-0.0016 + 9.6427i$	$-0.0082 + 9.6423i$	$-0.0163 + 9.6411i$
$z_2 = 10^3\times$	$-0.0016 - 9.6427i$	$-0.0082 - 9.6423i$	$-0.0163 - 9.6411i$
$z_3 = 10^3\times$	$-0.0000 + 9.4830i$	$0.0000 + 9.4830i$	$-0.0000 + 9.4831i$
$z_4 = 10^3\times$	$-0.0000 - 9.4830i$	$0.0000 - 9.4830i$	$-0.0000 - 9.4831i$
$z_5 = 10^3\times$	$0.0000 + 9.4830i$	$-0.0000 + 9.4830i$	$0.0000 + 9.4831i$
$z_6 = 10^3\times$	$0.0000 - 9.4830i$	$-0.0000 - 9.4830i$	$0.0000 - 9.4831i$
$z_7 = 10^3\times$	$-1.0000 + 0.0000i$	$-1.0000 + 0.0000i$	$-1.0001 + 0.0001i$
$z_8 = 10^3\times$	$-0.1000 + 0.0000i$	$-0.5000 + 0.0000i$	$-1.0001 - 0.0001i$
$z_9 = 10^3\times$	$-0.1000 + 0.0000i$	$-0.5000 - 0.0000i$	$-0.9999 + 0.0000i$
$z_{10} = 10^3\times$	$-0.0967 + 0.0000i$	$-0.4836 + 0.0000i$	$-0.9675 + 0.0000i$

In Fig. 24, the circle and cross symbols show the zeros and poles affected by the increasing of g_{mdis} in the condition of zero-pole cancellation and gain of system $\in [0, +\infty$. Obviously, the complex conjugate poles are getting far away to the negative half plane and close to the real axis, while the real poles are also getting far away from origin.

5.2.2 Cut–off frequency of LDOB

Secondly, reviewing the equations of last two sections.

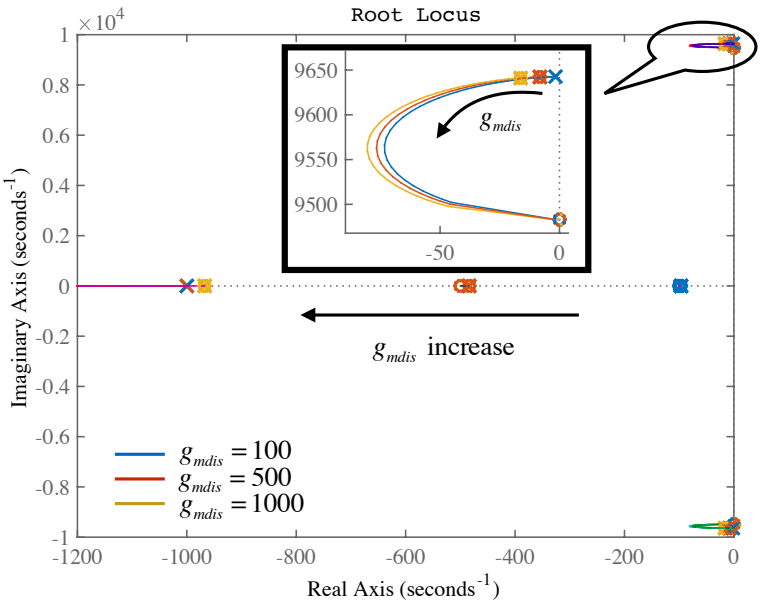

Fig. 24: Root Locus of feed–forward system using proposed controller. Parameter: $g_{mdis} = 100, 500, 1000\text{rad/s}$

$$H(s) = \alpha K_f \frac{J_m G_r^2 (J_l s^2 + K_s)(s + g_{mdis}) + J_l K_s s}{J_m G_r^2 (J_l s^2 + K_s)(s + g_{mdis}) + J_l K_s s + K_f J_m J_l K_s g_{mdis}} - \frac{K_s s(s + g_{ldis})}{J_m G_r g_{ldis} (J_l s^2 + K_s)(s + g_{mdis})} \tag{5-2}$$

The item of $(s + g_{ldis})$ is cancelled in the combination of Eq. (5-1) and (5-2). Therefore, the parameter g_{ldis} supposes no matter to stability of the system that is verified as Fig. 25.

Without the cancellation of zero-pole of $G_{BD}(s)$, the poles and zeros in the condition of $Kf = 1724$ are shown as follow, only one pole value p_7 is changed by g_{ldis}.

The circle and cross symbols show the zeros and poles affected by the increasing of g_{ldis}. The poles have no change of location.

5.2.3 Cut–off frequency of LPF

The last one, in Fig. 26, the circle and cross symbols show the zeros and poles affected by the increasing of g_{LPF}. The real poles have no change of location, while the complex conjugate poles are getting close to the imaginary axis.

Without the cancellation of zero-pole of $G_{BD}(s)$, the poles and zeros in the condition of $Kf = 1724$ are shown as follow. As same as the cut–off frequency of LDOB, only one pole value p_7 is changed by g_{LPF}.

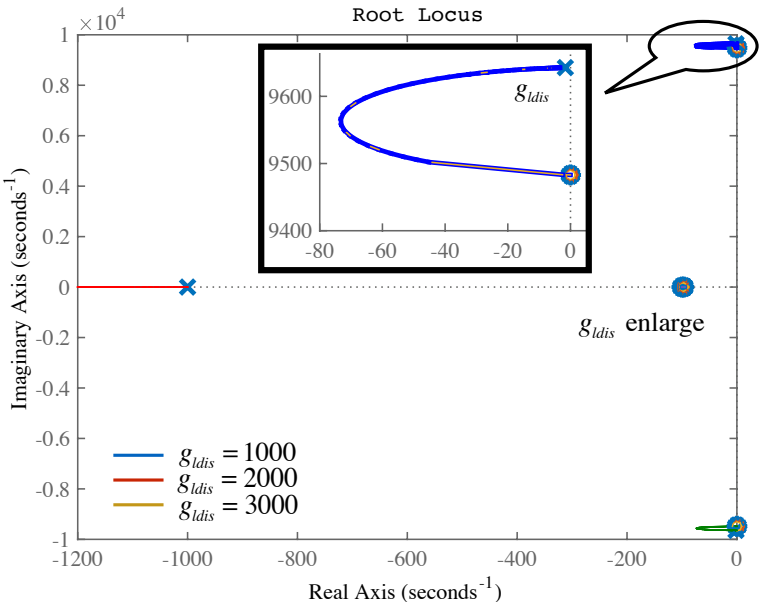

Fig. 25: Root Locus of feed–forward system using proposed controller. Parameter: $g_{ldis} = 1000, 2000, 3000$ rad/s

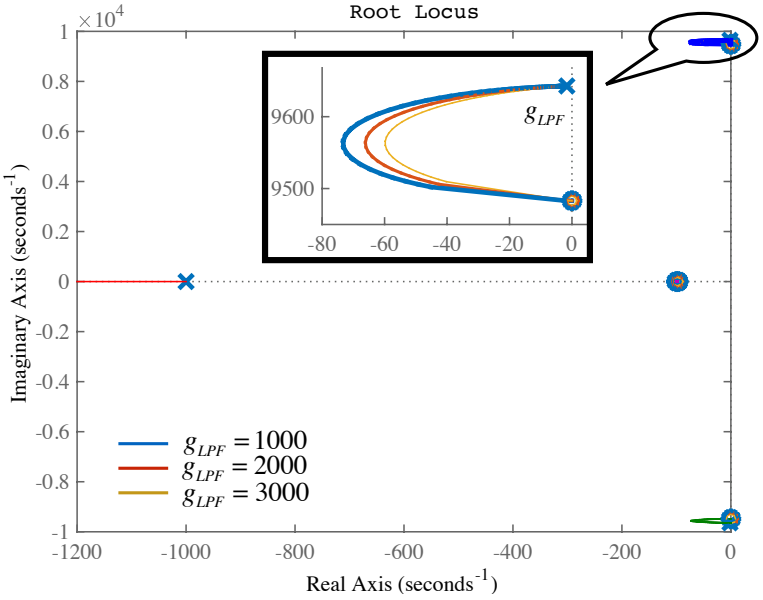

Fig. 26: Root Locus of feed–forward system using proposed controller. Parameter: $g_{LPF} = 1000, 2000, 3000$ rad/s

Therefore, the Fig. 25 and Fig. 26 show that if g_{ldis} and g_{LPF} are assumed as same value as 1000 rad/s, the system realizes better effect of vibration suppression. In addition, the parameter of g_{mdis} is playing a pair of contradictory roles that difficult to decide. The farther the complex conjugate poles are away from imaginary axis, the better for vibration suppression. At the same time, the real pole closer to origin is required for slowly decaying of components. Finally, by trial and error, the smaller value 100 rad/s is decided for g_{mdis}.

Tab. 6: Zero-poles in different g_{ldis}.

	$g_{ldis} = 1000$	$g_{ldis} = 2000$	$g_{ldis} = 3000$
$p_1 = 10^3\times$	$-0.0016 + 9.6427i$	$-0.0016 + 9.6427i$	$-0.0016 + 9.6427i$
$p_2 = 10^3\times$	$-0.0016 - 9.6427i$	$-0.0016 - 9.6427i$	$-0.0016 - 9.6427i$
$p_3 = 10^3\times$	$-0.0016 + 9.6427i$	$-0.0016 + 9.6427i$	$-0.0016 + 9.6427i$
$p_4 = 10^3\times$	$-0.0016 - 9.6427i$	$-0.0016 - 9.6427i$	$-0.0016 - 9.6427i$
$p_5 = 10^3\times$	$0.0000 + 9.4830i$	$-0.0000 + 9.4830i$	$-0.0000 + 9.4830i$
$p_6 = 10^3\times$	$0.0000 - 9.4830i$	$-0.0000 - 9.4830i$	$-0.0000 - 9.4830i$
$p_7 = 10^3\times$	$-1.0000 + 0.0000i$	$-2.0000 + 0.0000i$	$-3.0000 + 0.000i$
$p_8 = 10^3\times$	$-1.0000 + 0.0000i$	$-1.0000 - 0.0000i$	$-1.0000 + 0.0000i$
$p_9 = 10^3\times$	$-0.1000 + 0.0000i$	$-1.0000 + 0.0000i$	$-0.1000 + 0.0000i$
$p_{10} = 10^3\times$	$-0.0967 + 0.0000i$	$-0.0967 + 0.0000i$	$-0.0967 + 0.0000i$
$p_{11} = 10^3\times$	$-0.0967 + 0.0000i$	$-0.0967 + 0.0000i$	$-0.0967 + 0.0000i$
$z_1 = 10^3\times$	$-0.0016 + 9.6427i$	$-0.0016 + 9.6427i$	$-0.0016 + 9.6427i$
$z_2 = 10^3\times$	$-0.0016 - 9.6427i$	$-0.0016 - 9.6427i$	$-0.0016 - 9.6427i$
$z_3 = 10^3\times$	$-0.0000 + 9.4830i$	$0.0000 + 9.4831i$	$0.0000 + 9.4831i$
$z_4 = 10^3\times$	$-0.0000 - 9.4830i$	$0.0000 - 9.4831i$	$0.0000 - 9.4831i$
$z_5 = 10^3\times$	$0.0000 + 9.4830i$	$-0.0000 + 9.4830i$	$-0.0000 + 9.4830i$
$z_6 = 10^3\times$	$0.0000 - 9.4830i$	$-0.0000 - 9.4830i$	$-0.0000 - 9.4830i$
$z_7 = 10^3\times$	$-1.0000 + 0.0000i$	$-1.0000 + 0.0000i$	$-1.0000 + 0.0000i$
$z_8 = 10^3\times$	$-0.1000 + 0.0000i$	$-0.1000 + 0.0000i$	$-0.1000 + 0.0000i$
$z_9 = 10^3\times$	$-0.1000 + 0.0000i$	$-0.1000 - 0.0000i$	$-0.1000 - 0.0000i$
$z_{10} = 10^3\times$	$-0.0967 + 0.0000i$	$-0.0967 + 0.0000i$	$-0.0967 + 0.0000i$

5.3 Frequency characteristics of proposed back–drivability

In chapter 2.3.1, the equivalent inertia of both directions in geared two–inertia system are discussed in the condition of pure mechanical construction. In this section, the drivability of no control, the referenced forward drive control and the proposed back drive control are summarized based on the cases in Tab. 9 and parameters decided by previous section Tab. 8.

In Fig. 27, it shows the comparison of referenced forward–drivability $G_{FDL}(s)$, back–drivability with no control $G_B(s)$ and proposed back–drivability $G_{BDH}(s)$. It is clearly shown that, the frequency characteristics curve of proposed back–drivability $G_{BDH}(s)$ and referenced forward–drivability $G_{FDL}(s)$ overlap, at the same time, both appear to be convergence in high frequency and less frequency oscillation than purely mechanical control of back drive. It should be noted that, the better amplitude gain in $G_B(s)$ can not be considered as its real advantage due to the

Tab. 7: Zero-poles in different g_{LPF}.

	$g_{LPF} = 1000$	$g_{LPF} = 2000$	$g_{LPF} = 3000$
$p_1 = 10^3\times$	$-0.0016 + 9.6427i$	$-0.0016 + 9.6427i$	$-0.0016 + 9.6427i$
$p_2 = 10^3\times$	$-0.0016 - 9.6427i$	$-0.0016 - 9.6427i$	$-0.0016 - 9.6427i$
$p_3 = 10^3\times$	$-0.0016 + 9.6427i$	$-0.0016 + 9.6427i$	$-0.0016 + 9.6427i$
$p_4 = 10^3\times$	$-0.0016 - 9.6427i$	$-0.0016 - 9.6427i$	$-0.0016 - 9.6427i$
$p_5 = 10^3\times$	$0.0000 + 9.4830i$	$-0.0000 + 9.4830i$	$-0.0000 + 9.4830i$
$p_6 = 10^3\times$	$0.0000 - 9.4830i$	$-0.0000 - 9.4830i$	$-0.0000 - 9.4830i$
$p_7 = 10^3\times$	$-1.0000 + 0.0000i$	$-2.0000 + 0.0000i$	$-3.0000 + 0.000i$
$p_8 = 10^3\times$	$-1.0000 + 0.0000i$	$-1.0000 - 0.0000i$	$-1.0000 + 0.0000i$
$p_9 = 10^3\times$	$-0.1000 + 0.0000i$	$-1.0000 + 0.0000i$	$-0.1000 + 0.0000i$
$p_{10} = 10^3\times$	$-0.0967 + 0.0000i$	$-0.0967 + 0.0000i$	$-0.0967 + 0.0000i$
$p_{11} = 10^3\times$	$-0.0967 + 0.0000i$	$-0.0967 + 0.0000i$	$-0.0967 + 0.0000i$
$z_1 = 10^3\times$	$-0.0016 + 9.6427i$	$-0.0016 + 9.6427i$	$-0.0016 + 9.6427i$
$z_2 = 10^3\times$	$-0.0016 - 9.6427i$	$-0.0016 - 9.6427i$	$-0.0016 - 9.6427i$
$z_3 = 10^3\times$	$-0.0000 + 9.4830i$	$0.0000 + 9.4831i$	$0.0000 + 9.4831i$
$z_4 = 10^3\times$	$-0.0000 - 9.4830i$	$0.0000 - 9.4831i$	$0.0000 - 9.4831i$
$z_5 = 10^3\times$	$0.0000 + 9.4830i$	$-0.0000 + 9.4830i$	$-0.0000 + 9.4830i$
$z_6 = 10^3\times$	$0.0000 - 9.4830i$	$-0.0000 - 9.4830i$	$-0.0000 - 9.4830i$
$z_7 = 10^3\times$	$-1.0000 + 0.0000i$	$-1.0000 + 0.0000i$	$-1.0000 + 0.0000i$
$z_8 = 10^3\times$	$-0.1000 + 0.0000i$	$-0.1000 + 0.0000i$	$-0.1000 + 0.0000i$
$z_9 = 10^3\times$	$-0.1000 + 0.0000i$	$-0.1000 - 0.0000i$	$-0.1000 - 0.0000i$
$z_{10} = 10^3\times$	$-0.0967 + 0.0000i$	$-0.0967 + 0.0000i$	$-0.0967 + 0.0000i$

feature of open–loop control without gain parameter.

5.4 Step responses comparison of referenced forward drive and proposed back drive

In this section, the step responses comparison of referenced forward drive and proposed back drive are given based on the cases of Tab. 10 to discuss the steady–state response and transient response for both control.

Eq. (5-3) is the calculated amplitude of referenced forward–drivability and proposed back–drivability.

Tab. 8: Control parameters.

Nominal motor inertia	J_{mn}	5.8×10^{-8}	kgm^2
Nominal load inertia	J_{ln}	1.39×10^{-5}	kgm^2
Nominal torque constant of drive motor	K_{tn}	0.0139	N/A
Nominal torque constant of load motor	K_{tnl}	0.0302	N/A
Nominal connection constant	K_{sn}	1250	
Reducer ratio	G_r	84	
Torque gain	K_f	1724.1	
Cut-off frequency of DOB	g_{mdis}	100	rad/s
Cut-off frequency of LDOB	g_{ldis}	1000	rad/s
Cut-off frequency of LPF	g_{LPF}	1000	rad/s
Control period	T_s	0.1	ms
Scaling factor	α	1	

Tab. 9: Simulation comparison of bode diagram.

Sim. 1	$G_{FDL}(s)$	referenced forward–drivability
Sim. 2	$G_B(s)$	back–drivability w/o controller
Sim. 3	$G_{BDH}(s)$	proposed back–drivability

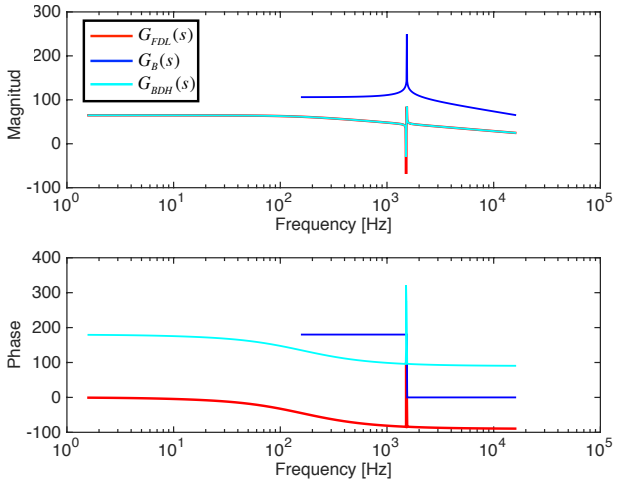

Fig. 27: Sim. 1, 2, 3: the comparison of bode diagram for each drivability in geared two–inertia system.

$$A_{G_{FDL}} = A_{G_{BDH}} \doteq 20log_{10}(\alpha K_f) = 64.7 \tag{5-3}$$

Tab. 10: Comparison of step responses for velocity and acceleration.

Sim. 4	referenced forward drive	$\tau_{cmd} = 0.05Nm\ (t < 1s)$
Sim. 5	proposed back drive	$\tau_l^{dis} = 0.05Nm\ (t < 1s)$

Cases of Tab. 10 are shown the simulation results as Fig. 28 and Fig. 29, the same acceleration

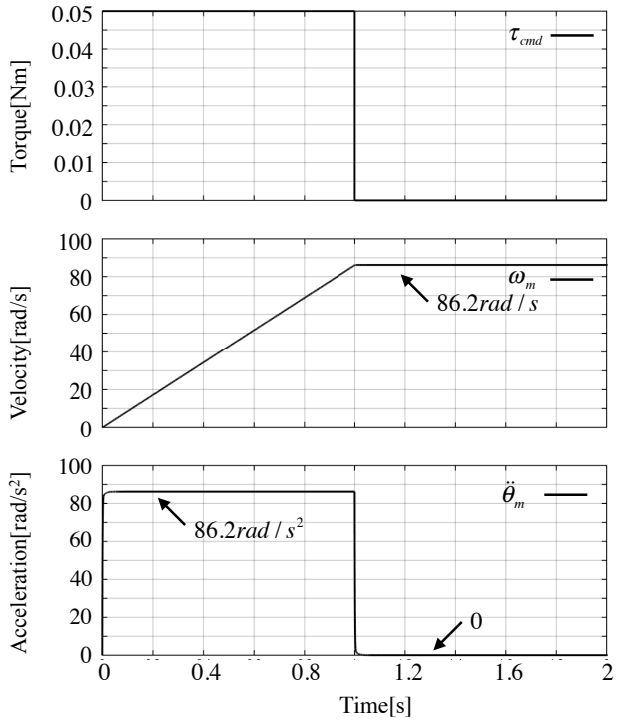

Fig. 28: Sim. 4: step response of velocity and acceleration for referenced forward drive.

of motor are realized in referenced forward–drive and proposed control. Both of forward and back drive are achieved 86.2 rad/s^2 of acceleration, which means as the same drivability as the bode diagram shown results.

5.5 Step responses comparison of referenced forward drive and proposed back drive

Since there is only g_{mdis} has a obvious effect on the stability and performance of the system in the above parametric analysis. In this section, the case of different g_{mdis} values are discussed based on following simulation cases of step response. The cases of Tab. 11 are given to discuss the steady–state response and transient response of acceleration in both forward drive and back drive.

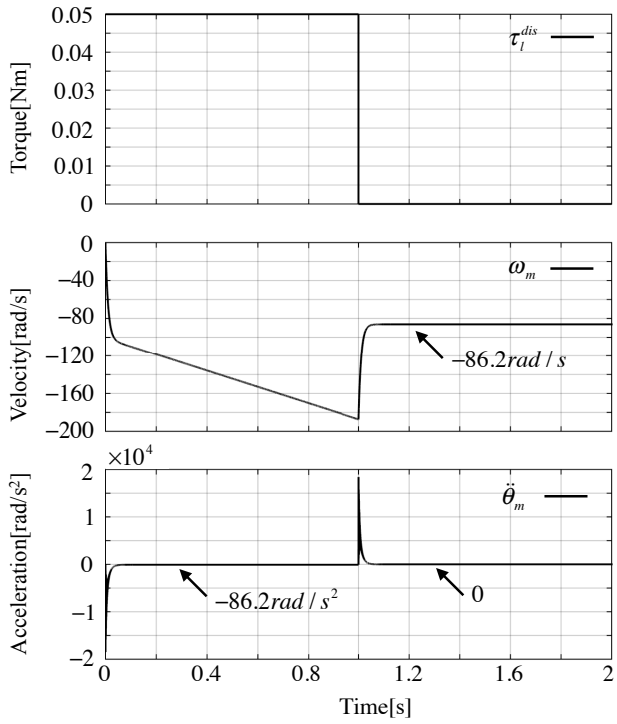

Fig. 29: Sim. 5: step response of velocity and acceleration for proposed back drive.

Tab. 11: Step responses of acceleration for different $g_{mdis} = 100, 500, 1000$ rad/s.

Sim. 6	$\ddot{\theta}_m$ of referenced forward drive	$\tau_{cmd} = 0.05Nm\ (t < 1s)$
Sim. 7	$\ddot{\theta}_m$ of proposed back drive	$\tau_l^{dis} = 0.05Nm\ (t < 1s)$

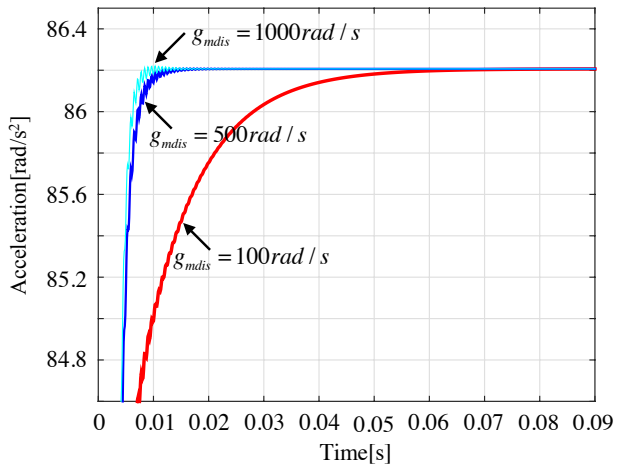

Fig. 30: Sim. 6: step response of acceleration for referenced forward drive.

Fig. 30 and Fig. 31(b) are shown the transient response of acceleration of motor in referenced forward drive and proposed back drive based on geared two–inertia system in the condition of input torque as 0.05 Nm, which are consistent with equation expressions of $G_{FDL}(s)$ and

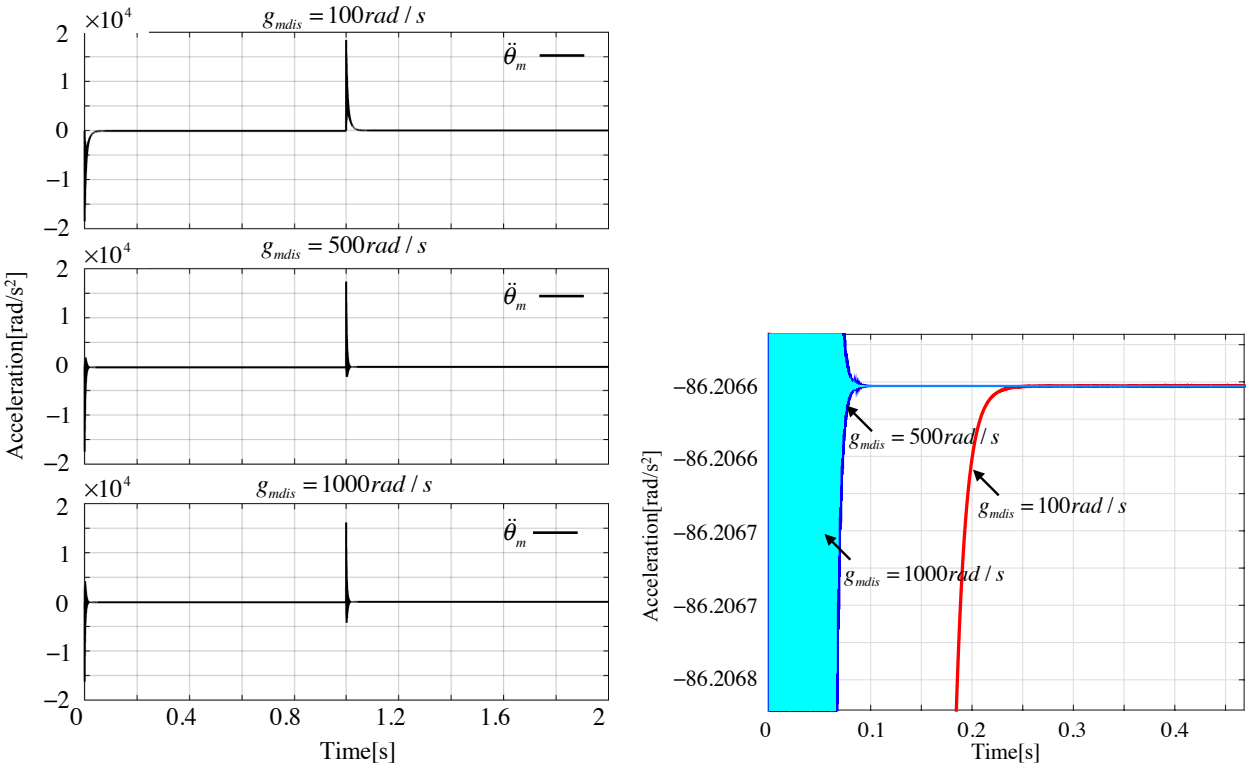

(a) review of step response. (b) transient response of acceleration.

Fig. 31: Sim. 7: step response of acceleration for proposed back drive.

Tab. 12: Summary of transient characteristics for referenced forward drive.

referenced forward drive	delay time t_d	rise time t_r	convergence time t_s ($< 2\%$)
$g_{mdis} = 100$rad/s	0.0007s	0.1462	0.0132s
$g_{mdis} = 500$rad/s	0.0007s	0.0543	0.0051s
$g_{mdis} = 1000$rad/s	0.0007s	0.0409	0.0047s

$G_{BDH}(s)$. It is clearly seen that in referenced forward drive, the higher the g_{mdis}, the shorter the rise time of the system and the faster the response. However, in the condition of $g_{mdis} = 1000$ rad/s, the overshoot and oscillation occur.

Tab. 12 is the summary of transient response of acceleration for referenced forward drive in different g_{mdis}. Three parameters in the overdamping case were selected to present the transient characteristics under this simulation. It can be found that transient characteristics are getting better as g_{mdis} getting bigger.

At the same time, in proposed back drive, as the g_{mdis} increases, the transient characteristics of the system are the same as the forward drive, but much deteriorated than forward drive. Tab. 13 is the summary of transient response of acceleration for proposed back drive in different g_{mdis}. Three parameters in the overshoot case were selected to present the transient charac-

Tab. 13: Summary of transient characteristics for proposed back drive.

proposed back drive	peak time t_p	maximum overshoot M_p	convergence time t_s ($< 2\%$)
$g_{mdis} = 100$rad/s	0.0002s	21370%	0.0973s
$g_{mdis} = 500$rad/s	0.0002s	20161%	0.0352s
$g_{mdis} = 1000$rad/s	0.0002s	18762%	0.0337s

Tab. 14: Step responses of velocity for different $g_{mdis} = 100, 500, 1000$ rad/s.

Sim. 8	ω_m of referenced forward drive	$\tau_{cmd} = 0.05Nm$ $(t < 1s)$
Sim. 9	ω_m of proposed back drive	$\tau_l^{dis} = 0.05Nm$ $(t < 1s)$

teristics under this simulation. It can be found that the convergence time is getting shorter according to increasing of g_{mdis}, while maximum overshooting is getting smaller. Even if the system converges around the time value of 0.1s, the severe overshooting occur in all g_{mdis}, however, oscillation are even more unexpected for back drive in the condition of $g_{mdis} = 500, 1000$ rad/s. As a result, the forward drive is allowed higher g_{mdis} to realize better transient characteristics than proposed back drive.

In order to validate the above results, the cases of Tab. 14 are given to discuss the steady–state response and transient response of velocity in both forward drive and back drive.

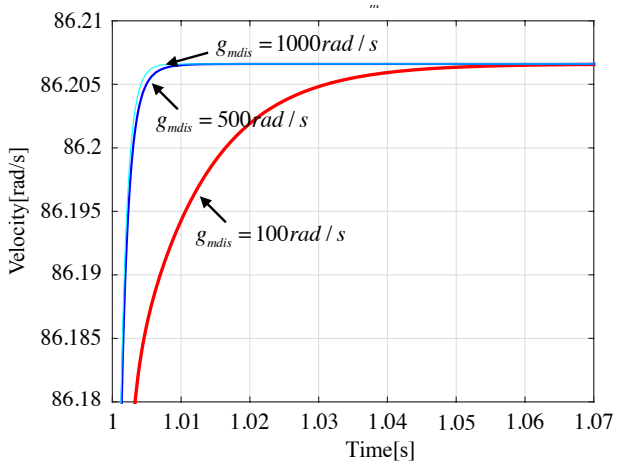

Fig. 32: Sim. 8: step response of velocity for referenced forward drive.

Fig. 32 and Fig. 33 are shown the transient response of velocity of motor in forward drive and back drive based on geared two–inertia system. It is clearly seen that in forward drive, the higher the g_{mdis}, the shorter the rise time of the system and the faster the response, even if in the condition of $g_{mdis} = 1000$ rad/s.

At the same time, in back drive, in the condition of $g_{mdis} = 500, 1000$ rad/s, due to the

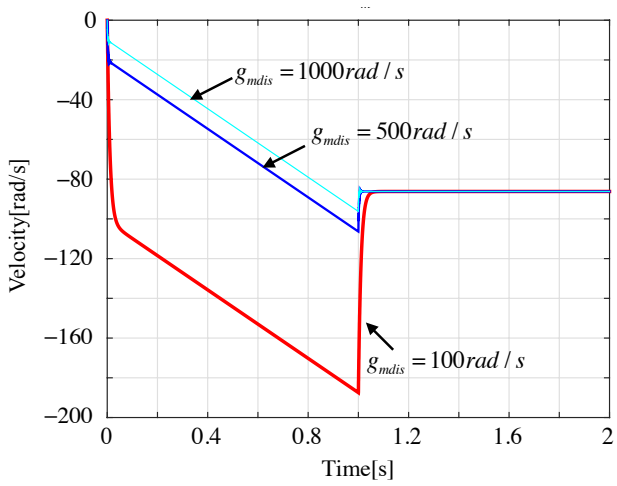

Fig. 33: Sim. 9: step response of velocity for proposed back drive.

overshoot and oscillation of the acceleration, the increasing of the velocity of the system is slower than in the case of $g_{mdis} = 100$ rad/s instead.

In summary, the selection of $g_{mdis} = 100$ rad/s is expected for proposed back drive.

5.6 Summary of this chapter

In this chapter, The stability of proposed control method with DOB, LDOB and designed controller based on parameters identification are discussed. Based on the steady–state response and transient response in simulations, the parameters of $g_{mdis} = 100 rad/s, g_{ldis} = g_{LPF} =$ 1000 rad/s are selected for later discussions.

Chapter 6

Discretization of Controller $H(s)$

6.1 Introduction

According to above discussion theoretically in last chapter, back–drivability as Eq. (4-11) is suppose to realize not only same amplitude but also dynamic characteristic with the forward–drivability with low–pass filter as Eq. (4-7) in the condition of $\alpha = 1$.

Nevertheless, in experiments, the controller $H(s)$ is described in C programming. Since the designed controller is too complicated to realize factorisation, the signal discretization is applied to motion control, which is given in this chapter.

6.2 Discretizetion method

Commonly there are three types of discretisation methods widely applied. Forward difference method, backward difference method and bilinear transform (Tustin transform). Forward difference method could not guarantee the system stability by discretisation. Backward difference method is easy to calculated and could realise the stability of system if the original continues system is stable, but distortion of frequency response and process characteristics are occurred due to the low–pass filter in original continues system. In this thesis, Tustin transform is utilised. The transform principle is shown as Eq. (6-1),

$$s = \frac{2}{T_s}\frac{1 - z^{-1}}{1 + z^{-1}} \tag{6-1}$$

where:

s: operator of continuous signal

z: operator of discrete signal

T_s: sampling period of discretization

The discretized controller is suppose to be expressed as Eq. (6-2) with discrete operator,

$$H(z) = \frac{b_{dH0} + b_{dH1}z^{-1} + b_{dH2}z^{-2} + \cdots b_{dH6}z^{-6}}{a_{dH0} + a_{dH1}z^{-1} + a_{dH2}z^{-2} + \cdots a_{dH6}z^{-6}} \tag{6-2}$$

where:

$a_{dH0}, a_{dH1}, ...$: parameters of each order of discrete integral operator, the numerical subscript denotes the order

$b_{dH0}, b_{dH1}, ...$: parameters of each order of discrete differential operator, the numerical subscript denotes the order

$z^{-1}, z^{-2}, ...$: periods of signal delay, the numerical supscript denotes how many periods delayed

Then the discretised input signal $H(z)$ is expressed as Eq. (6-4).

$$H(z) = 1 + (m_2(z)z^{-1} + m_1(z))z^{-1} \tag{6-3}$$

where :

$$m_2(z) = b_2 - a_2U(z)$$
$$m_1(z) = b_1 - a_1U(z)$$

$m_1(z), m_2(z)$ are intermediate variables during the calculation in each delay. According to above formulas, the Discretised controller $H(z)$ is achieved by series algorithm shown as Fig. 34.

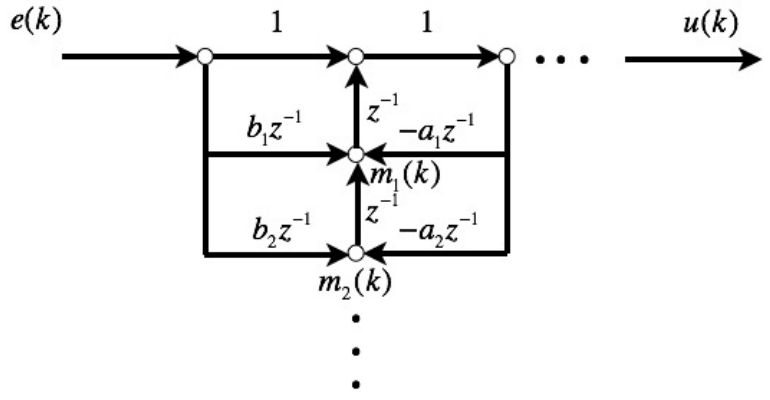

Fig. 34: Series algorithm for realising discretised controller.

From this figure, $m_1(k), m_2(k)$ denote the joint of each layer of delay. The discretised output signal is calculated via this series algorithm of layer–by–layer recursive.

6.3 Discretization of $H(s)$

In this section, the discratization of controller $H(s)$ is given in two versions. First, since the full orders of representation of back–drivability would be kept (Higher components in brackets

are not zero.), and take part in the discretization, as a result, the expected effect on the system considered from full version in discretized controller $H(z)$ are as follow as Eq. (6-4).

$$\|H(e^{j\omega})\| = \sqrt{\frac{(\frac{b_{dH0}}{a_{dH0}})^2 + \cdots (\frac{b_{dH6}}{a_{dH0}})^2 + 2(\frac{b_{dH0}b_{dH1}}{a_{dH0}^2} + \cdots \frac{b_{dH5}}{b_{dH6}}a_{dH0}^2)cos(\omega) + 2(\frac{b_{dH0}b_{dH1}}{a_{dH0}^2} + \cdots \frac{b_{dH4}b_{dH6}}{a_{dH0}^2})cos(2\omega)\cdots}{1 + (\frac{a_{dH1}}{a_{dH0}})^2 + \cdots (\frac{a_{dH6}}{a_{dH0}})^2 + 2(\frac{a_{dH1}}{a_{dH0}} + \cdots \frac{a_{dH5}a_{dH6}}{a_{dH0}^2})cos(\omega) + 2(\frac{a_{dH2}}{a_{dH0}} + \cdots \frac{a_{dH4}a_{dH6}}{a_{dH0}^2})cos(2\omega)\cdots}} \tag{6-4}$$

In order to focus the discussion on scaling factor α, another impact factor K_f is suppose to be decided. Since the input torque can not be selected too big in consideration of gear ratio, the torque gain of forward–drive is decided as the 0.0001 multiple of $1/J_m$ ($K_f = 1724.1$) to simplified the calculation. So that, considering the full real items, the amplitude of $H(z)$ is as Eq. (6-5).

$$A_{G_{H(z)}} = 20log_{10}(\sqrt{\frac{b_{dH0}^2 + b_{dH1}^2 + \cdots + b_{dH6}^2}{a_{dH0}^2 + a_{dH1}^2 + \cdots + a_{dH6}^2}}) = 20log_{10}(Kf\sqrt{\alpha^2 + 3.814\alpha + 155.45^2} \tag{6-5}$$

The Schematic diagram of amplitude of above equation is as follow Fig. 35:

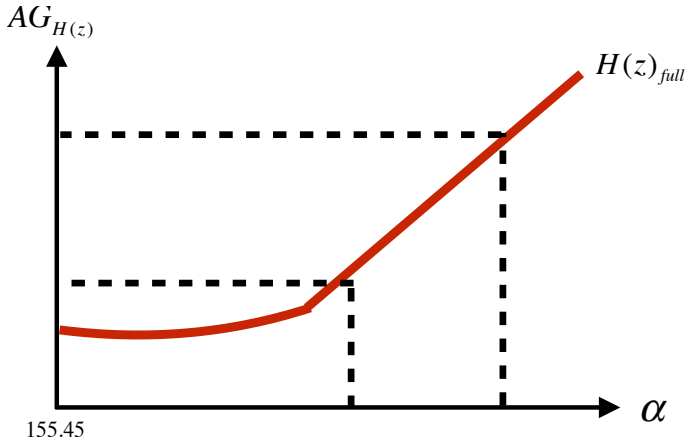

Fig. 35: Schematic diagram of amplitude of full version of $H(z)$.

From this figure, in the case of $\alpha < 155.45$, the amplitude of $H(z)$ does not change clearly. There is also nonlinear part during the value larger than 155.45 and a certain value. In addition, the calculation of Eq. (6-5) is quite complicate for author, a simplified version of amplitude of $H(z)$ is given. As a result, the expected effect on the system considered from constant items in discretized controller $H(z)$ are as follow Eq. (6-7).

$$
\begin{aligned}
b_{dH0} &= b_{H6}(\frac{2}{T_s})^6 + b_{H5}(\frac{2}{T_s})^5 + b_{H4}(\frac{2}{T_s})^4 + b_{H3}(\frac{2}{T_s})^3 \\
&\quad + b_{H2}(\frac{2}{T_s})^2 + b_{H1}\frac{2}{T_s} + b_{H0}, \\
a_{dH0} &= a_{H6}(\frac{2}{T_s})^6 + a_{H5}(\frac{2}{T_s})^5 + a_{H4}(\frac{2}{T_s})^4 + a_{H3}(\frac{2}{T_s})^3 + \\
&\quad a_{H2}(\frac{2}{T_s})^2 + a_{H1}\frac{2}{T_s} + a_{H0} \qquad \text{(6-6)}
\end{aligned}
$$

$$
\begin{aligned}
A_{G_{H(z)}} &= 20log_{10}(\sqrt{\frac{b_{dH0}^2}{a_{dH0}^2}}) = 20log_{10}(Kf\sqrt{\alpha^2 - 3913.2\alpha + 2088636}) \\
&= 20log_{10}(Kf\sqrt{(\alpha - 461.72)(\alpha - 451.27)}) \doteq 20log_{10}(Kf(\alpha - 456.6)) \qquad \text{(6-7)}
\end{aligned}
$$

The Schematic diagram of amplitude of above equation is as follow Fig. (36):

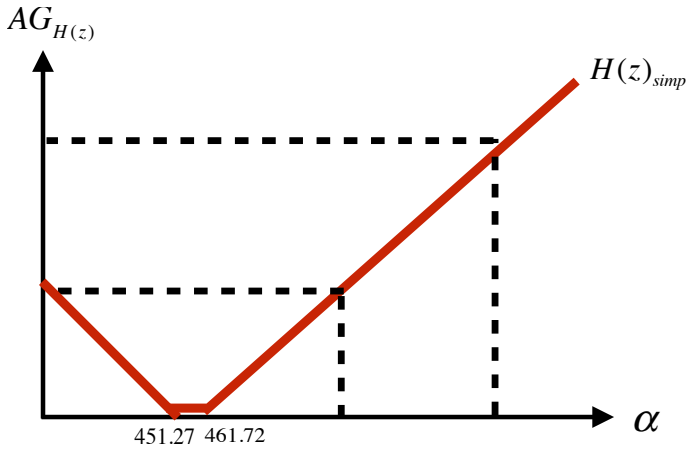

Fig. 36: Schematic diagram of amplitude of simplified version of $H(z)$.

From this figure, in the case of $\alpha \doteq 456.6$, the amplitude of $H(z)$ realizes the lowest value. For simplified the consideration of linear part of amplitude, the $\alpha_0 = 456.6$ as standard adjusted interval and $2\alpha_0 = 913.2$ as the starting scaling will be choose to later research.

6.4 Summary of this chapter

In this chapter, the discrete $H(s)$ are discussed in full version and simplified version. In the situation of this research, the simplified way are enough to design the the scaling factor and simplified the calculation. In next chapter, the other parameters of cut–off frequencies and range of scaling factor are discussed.

Chapter 7

Stability Statement and Analysis for α

7.1 Introduction

In previous two chapters, the proposed back–drive control are discussed in detail. The selection of parameter α can affect the stability and performance of the system which need to consider in both continuous system and discrete system. In this chapter,the stability statement and the discussion of parameter α is in progress.

7.2 Stability analysis

The stability of system is an important indicator for evaluation of constructing a controller. For discussion of stability of proposed control system, firstly, the dynamics of proposed control motion is summarized in follow equivalent block diagram and equation.

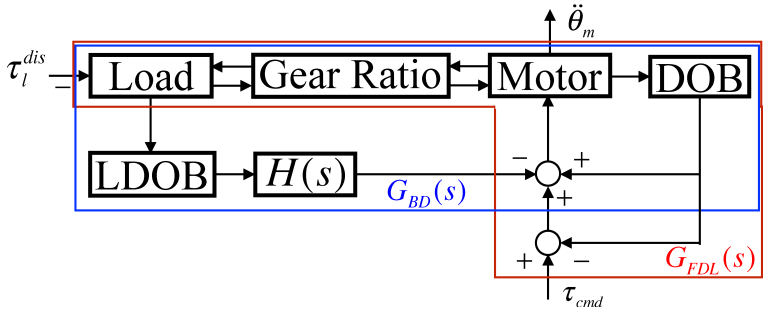

Fig. 37: Equivalent block diagram of full dynamics.

$$\ddot{\theta}_m = \begin{bmatrix} G_{FDL}(s) & 0 \\ 0 & G_{BD}(s) \end{bmatrix} \begin{bmatrix} \tau_{cmd} \\ \tau_l^{dis} \end{bmatrix} \tag{7-1}$$

Fig. 37 is the equivalent block diagram of in the condition of both referenced forward control and proposed back–drive control. In this figure, the control blocks in the red frame is the referenced forward dynamics with DOB and feedback control, while the control blocks in the blue frame is the proposed back–drive dynamics in this thesis. Obviously, the proposed back–drive dynamics includes an inner loop of DOB for compensation and a feed–forward loop to motor with designed controller $H(s)$.

In the view of expressions, Eq. (7-1) shows the full dynamics descriptions of proposed control method. In this research, the authors only discussed the situation of load side disturbance torque input while $\tau_{cmd} = 0$.

Feed-forward control is an open-loop control method based on disturbance that is often a command signal from an external operator. It responses to control signal in a pre-defined way without responding to how the motor reacts. It is able to operate at high speed and accuracy only if the mathematic model is designed with high quality.

On the account of the proposed control in this thesis is a feed-forward control, the stability of control system with proposed controller is restricted by hardware conditions which will discussed in later chapter. However, even if there is no physical meaning to discuss the stability in this thesis, the three parameters of cut-off frequency matter the stability and robustness of the proposed system.

7.3 Range of scaling factor

In this thesis, the performance of back–drivability that is evaluated via speed variation intuitively is discussed based on parameter of scaling factor α. Obviously, the item of α affects only numerator of the expression in the combination of Eq. (5-1) and (5-2). Therefore, the scaling factor α supposes no matter to stability of system that is verified as Fig. 38.

Actually, theoretically the scaling factor α looks like an unrestricted parameter, it does have limitation of selection based on experimental results. Even if the scaled up input torque from external to feed–forward to motor, the driver of motor could not generate enough current to follow it. Therefore, once the scaling factor is selected larger than the driving ability of motor, the back–driving system would keep the limited maximum velocity of motor and be out of control. In experimental setup, the drive motor has the restricted velocity at about 750 rad/s because of velocity protection of motor driver. Based on this situation, the range of scaling factor is selected under the limitation of max velocity as $\alpha < 9\alpha_0 = 4109.4$.

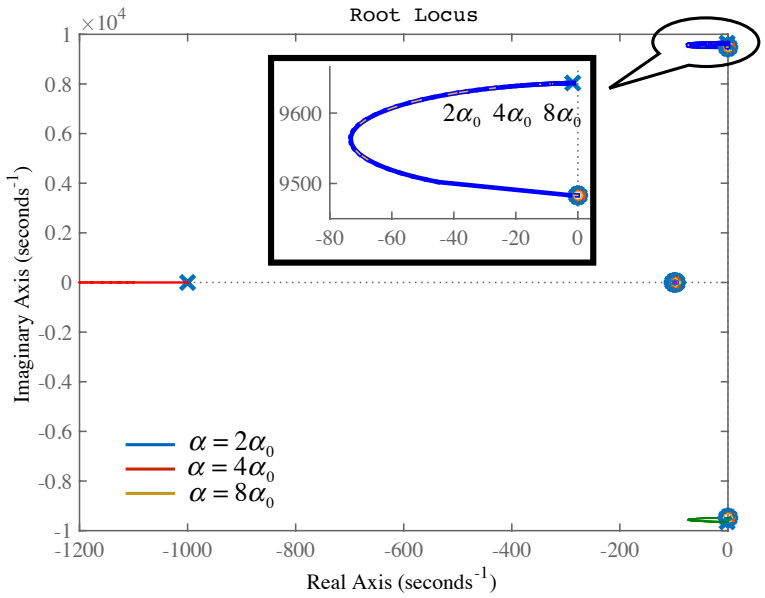

Fig. 38: Root Locus of feed–forward system using proposed controller. Parameter: $\alpha = 2\alpha_0, 4\alpha_0, 8\alpha_0$

7.4 Step responses comparison for proposed back drive in both continuous and discrete systems

Since there is α also has a obvious effect on the stability and performance of the system in the above parametric analysis. In this section, the case of different α values are discussed based on following simulation and experiment cases of step response. In both continuous and discrete systems and parameters decided by previous section Tab. 15.

7.4.1 Proposed continuous back drive system

The cases of Tab. 16 are given to discuss the steady–state response and transient response of acceleration and velocity for continuous back drive system in the different $\alpha = 1, 2, 4$.

Fig. 39(b) and Fig. 40 are shown the transient response of acceleration and velocity of motor in back drive based on geared two–inertia system in the condition of input torque as 0.05 Nm. It is clearly seen that in proposed back drive, whatever the α value is, the transient characteristics are shown as the severe overshooting and oscillation even if the system converges around the time value of 0.1s.

Tab. 13 is the summary of transient response of acceleration for proposed back drive in different α. Three parameters in the overshoot case were selected to present the transient characteristics under this simulation. It can be found that the parameter α does not effect on convergence time a lot. The maximum overshoot is reduced as α getting bigger.

Tab. 15: Control parameters.

Nominal motor inertia	J_{mn}	5.8×10^{-8}	kgm^2
Nominal load inertia	J_{ln}	1.39×10^{-5}	kgm^2
Nominal torque constant of drive motor	K_{tn}	0.0139	N/A
Nominal torque constant of load motor	K_{tnl}	0.0302	N/A
Nominal connection constant	K_{sn}	1250	
Reducer ratio	G_r	84	
Torque gain	K_f	1724.1	
Cut-off frequency of DOB	g_{mdis}	100	rad/s
Cut-off frequency of LDOB	g_{ldis}	1000	rad/s
Cut-off frequency of LPF	g_{LPF}	1000	rad/s
Control period	T_s	0.1	ms
Standard scaling factor for continuous system	α	1	
Standard scaling factor for discrete system	α_0	456.6	

Tab. 16: Comparison of step responses for velocity and acceleration for different $\alpha = 1, 2, 4$.

Sim. 1	$\ddot{\theta}_m$ of proposed back drive	$\tau_l^{dis} = 0.05Nm\ (t < 1s)$
Sim. 2	ω_m of proposed back drive	$\tau_l^{dis} = 0.05Nm\ (t < 1s)$

In Fig. 40, during the time period of input torque loading, the system consistently outputs much higher speed than expected (the speed after $1s$) due to oscillations and overshoots in acceleration. Moreover, as the α increases, the increasing of the velocity of the system is faster because of the value α equivalents to input torque gain. In summary, the α causes overshooting and oscillation in proposed back drive at transient response then system always in the situation of overshoot.

7.4.2 Proposed discrete back drive system

In the previous chapter, after calculating the conversion relationship in the value of α in the discrete system , the effect on the proposed discrete back drive system is discussed in this section. Since the discrete back drive is also the control systems used in the experiments, combined with the parametric analysis of g_{mdis} and g_{ldis} in the previous two chapters, an experiments that combines α, g_{mdis} and g_{ldis} (g_{LPF} is not discussed since it shows the same frequency characteristics as g_{ldis}) are given as the cases of Tab. 18 based on parameters of Tab. 15.

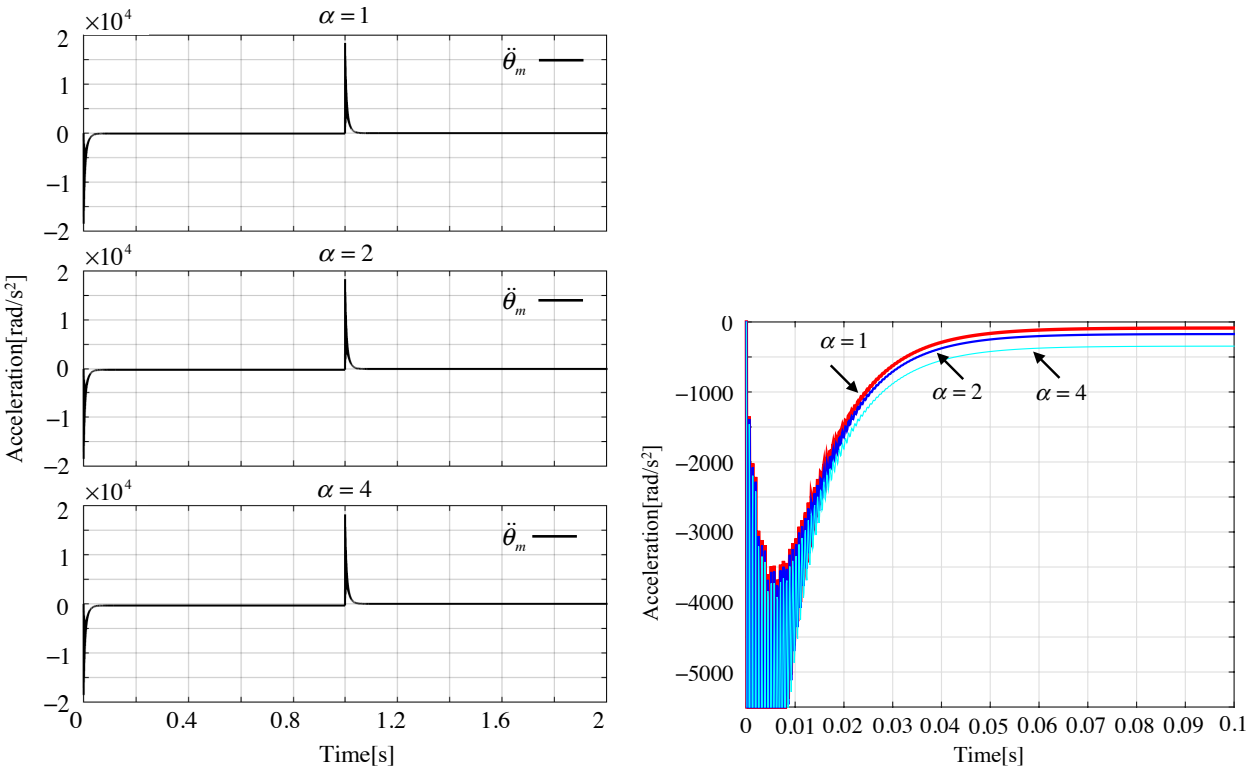

(a) review of step response.

(b) transient response of acceleration.

Fig. 39: Sim. 1: step response of acceleration for proposed back drive.

Tab. 17: Summary of transient characteristics for proposed back drive.

proposed back drive	peak time t_p	maximum overshoot M_p	convergence time t_s ($< 2\%$)
$\alpha = 1$	0.0003s	21370%	0.0973s
$\alpha = 2$	0.0003s	10647%	0.0903s
$\alpha = 4$	0.0003s	5286%	0.0825s

The nominal torque constant of load motor K_{tnl} is implemented. Via this design, the external torque input can be set as a constant value by the load motor from Eq. (7-2).

$$\tau_l^{dis} = K_t I_t = 0.05(Nm) \tag{7-2}$$

Fig. 41 show the velocity responses of motor in proposed back drive based on geared two–inertia system in the condition of input torque as 0.05 Nm for different g_{mdis} and g_{ldis}. In comparison with the simulated velocity response in chapter 5.4, the amplitude response of the velocity is lower than the simulation result due to the model parameter error in the experiment and the friction not considered in the simulation (the simulation result is -86.2rad/s, the experimental result is probably -70rad/s) shown as Fig. 41 (a).

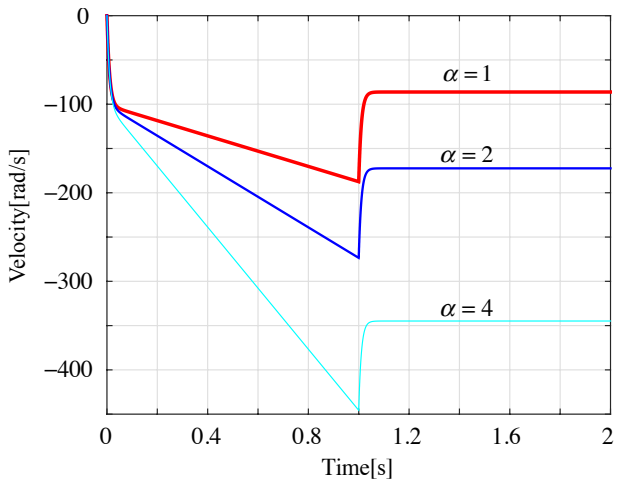

Fig. 40: Sim. 2: step response of velocity for proposed back drive.

Tab. 18: Comparison of step responses for velocity for $\alpha = 2\alpha_0$.

Exp. 1	$\tau_l^{dis} = 0.05Nm\ (t < 1s)$	$g_{mdis} = 100, 500, 1000\text{rad/s}$
Exp. 2	$\tau_l^{dis} = 0.05Nm\ (t < 1s)$	$g_{ldis} = 1000, 2000, 3000\text{rad/s}$

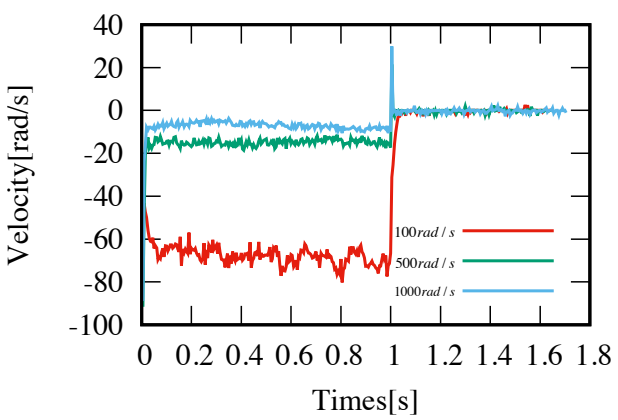

(a) velocity response of Exp.1.

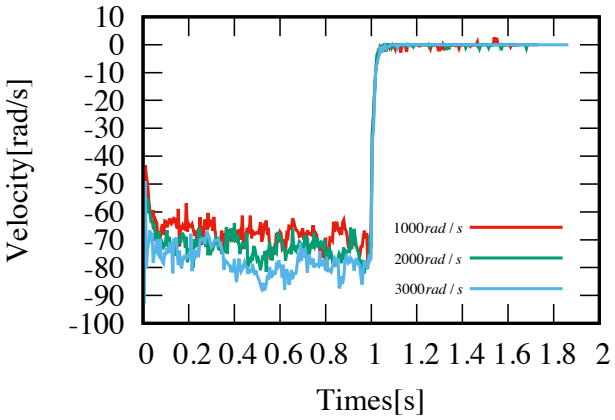

(b) velocity response of Exp.2.

Fig. 41: Exp. 1, 2: velocity response for proposed back drive in the condition of $\alpha = 2\alpha_0$.

On the other hand, as the same as the transient feature as simulation results in chapter 5.5, in the condition of $g_{mdis} = 500, 1000$ rad/s, due to the overshoot and oscillation of the acceleration, the increasing of the velocity of the system is slower than in the case of $g_{mdis} = 100$ rad/s instead.

In Fig. 41(b), as the frequency characteristics discussion in chapter 5.2.2, g_{ldis} has little effect on the velocity amplitude of the system. In the experiment, the increase of g_{ldis} brings a corresponding increase in the system output velocity, which is believed to be caused by oscillations and overshoot of the acceleration in the transient response.

Another experiments with another value of α are given as the cases of Tab. 19 as following.

Tab. 19: Comparison of step responses for velocity for $\alpha = 4\alpha_0$.

Exp. 3	$\tau_l^{dis} = 0.05Nm\ (t < 1s)$	$g_{mdis} = 100, 500, 1000\text{rad/s}$
Exp. 4	$\tau_l^{dis} = 0.05Nm\ (t < 1s)$	$g_{ldis} = 1000, 2000, 3000\text{rad/s}$

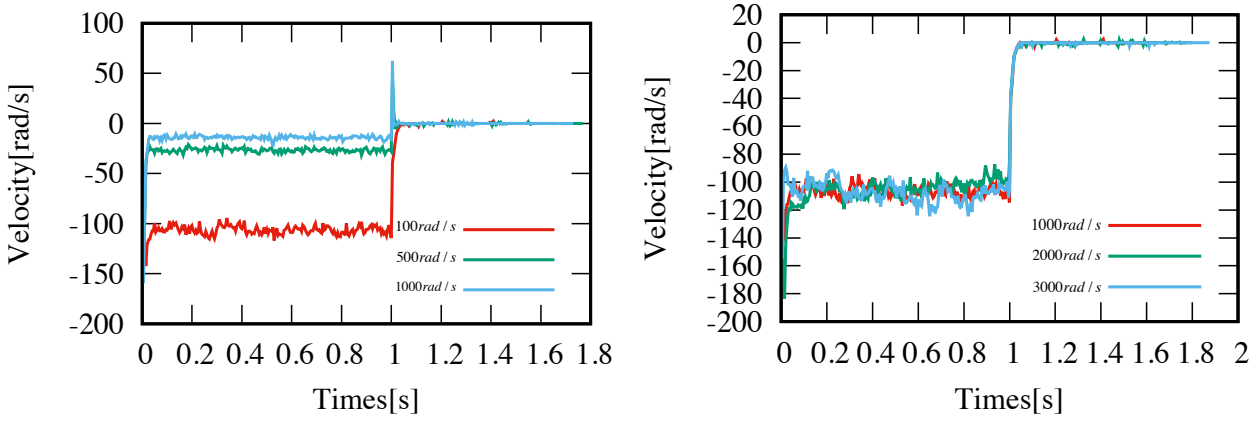

(a) velocity response of Exp.3.

(b) velocity response of Exp.4.

Fig. 42: Exp. 3, 4: velocity response for proposed back drive in the condition of $\alpha = 4\alpha_0$.

Fig. 42 show the velocity responses of motor in proposed back drive in the condition of $\alpha = 4\alpha_0$. Similar to the simulation results in the previous section, the change of α does not have much effect on the steady–state and transient characteristics of the system, but plays a gain role on the magnitude of the output velocity.

7.4.3 Limitation of α for mechanical reason

Based on the simulation and experimental results for α in the previous section, we find that the parameter α does not have much effect on the steady–state and transient characteristics of the system, and equivalent to an effect on the output amplitude gain of the system. According to this conclusion, theoretically the parameter α can be limited to the maximum speed of the motor only.

In practice, however, according to the analysis of the mechanical selection of the system mentioned in chapter 2.4.2, the angle sensor of the load–side motor is at least G_r times higher than that of the drive motor in order to achieve the same degree of sampling resolution for the drive motor and the load motor due to the presence of the gearbox. Due to hardware limitations, higher-resolution angle sensors are very expensive, so there is an interdependence between the parameter α and the gearbox ratio.

The detailed experimental validation about the take of parameter α will be given later in the experiment based on the hardware limitation.

7.5 Summary of this chapter

In this chapter, the stability of proposed control method and detailed discussion about the take of parameter α are given. Both in simulation and experiment results, the parameters $\alpha = [2\alpha_0, 8\alpha_0]$ are selected.

Chapter 8

Experiments

8.1 Introduction

In chapter 2.4, the experimental setup of geared two–inertia system is describes in detail the experimental devices, as well as the hardware equipments. In this chapter, related experiments of comparison evaluations with conventional method In chapter 3, the drivability comparison with referenced forward drive and back drive, and limitation of taking α will be in progress.

8.2 Experimental setup

In chapter 2.4, the experimental setup of geared two–inertia system is describes in details. In experiments, the overview of proposed control method is shown as Fig. 43. The execution of implementing the experiment by hand is supposed as Fig. 44, which is input by load motor instead. The utilized parameters refer to Tab. 20.

8.3 Comparison of conventional and proposed back–drivability

In this section, the effect of scaling factor α is discussed in proposed control and compared with conventional method by changing torque gain C_t. Case 1 shown in Tab. 21 is given in a constant torque input for different performance of back–drivability. The input torque is given during t=0–1s.

Fig. 45 is the group of velocities in different torque gain while Fig. 47 is the groups of velocities in different scaling factor. We are going to discuss the back–drivability in term of conventional method which is defined from the load–side torque to velocity of load. When the torque gain is selected as lower values from $\frac{1}{20J_m}$ to $\frac{1}{2J_m}$ (Author selected torque gain as $\frac{1}{20J_m}$ in conventional

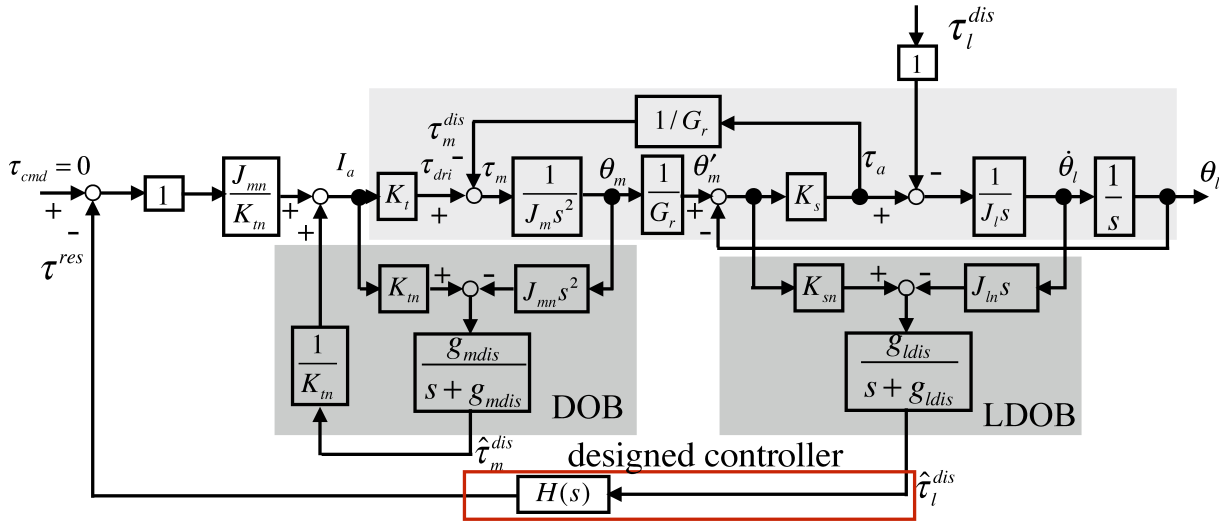

Fig. 43: Block diagram of proposed back drive with designed controller.

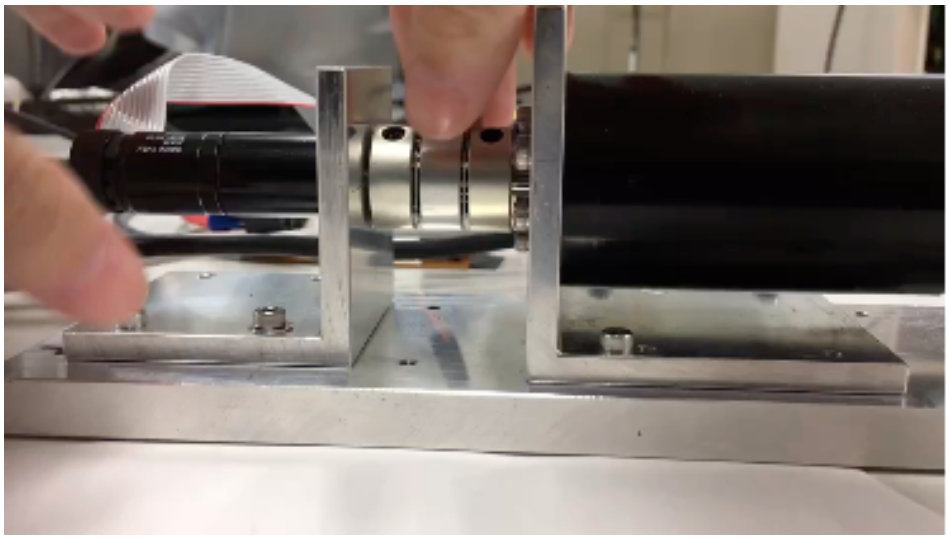

Fig. 44: Drive execution for back drive by hand.

method.), the velocity of load is increased little. However, keeping on largen the gain to $\frac{1}{J_m}$, the load velocity is improved a lot with un–clarified proportional and accompanied by oscillation.

It is easy to see the back–drivability performance plot in 3D figure in Fig. 46. From the figure, the performance of back–drivability in conventional method is displayed as a broken line shown as the black one with arrow since the un–clarified proportion of torque gain C_t.

In contrast, the load velocity of proposed method is proportionally increased along with the scaling factor as Fig. 48.

In Fig. 48, the approximate exponential line of improving of back–drivability is shown as red one with arrow.

This is the discussion of comparison of back–drivability improvement between conventional

Tab. 20: Control parameters.

Nominal motor inertia	J_{mn}	5.8×10^{-8}	kgm^2
Nominal load inertia	J_{ln}	1.39×10^{-5}	kgm^2
Nominal torque constant of drive motor	K_{tn}	0.0139	N/A
Nominal torque constant of load motor	K_{tnl}	0.0302	N/A
Nominal connection constant	K_{sn}	1250	
Reducer ratio	G_r	84	
Torque gain	K_f	1724.1	
Cut-off frequency of DOB	g_{mdis}	100	rad/s
Cut-off frequency of LDOB	g_{ldis}	1000	rad/s
Cut-off frequency of LPF	g_{LPF}	1000	rad/s
Control period	T_s	0.1	ms
Standard scaling factor	α_0	456.6	

Tab. 21: Comparison of back–drivability in conventional and proposed method.

Exp. 1	conventional control	$\tau_l^{dis} = -0.05Nm$	$C_t = 0.05/J_m, 0.1/J_m, 0.2/J_m, 0.5/J_m, 1/J_m$
Exp. 2	proposed control	$\tau_l^{dis} = -0.05Nm$	$\alpha = 2\alpha_0, 4\alpha_0, 6\alpha_0, 8\alpha_0$

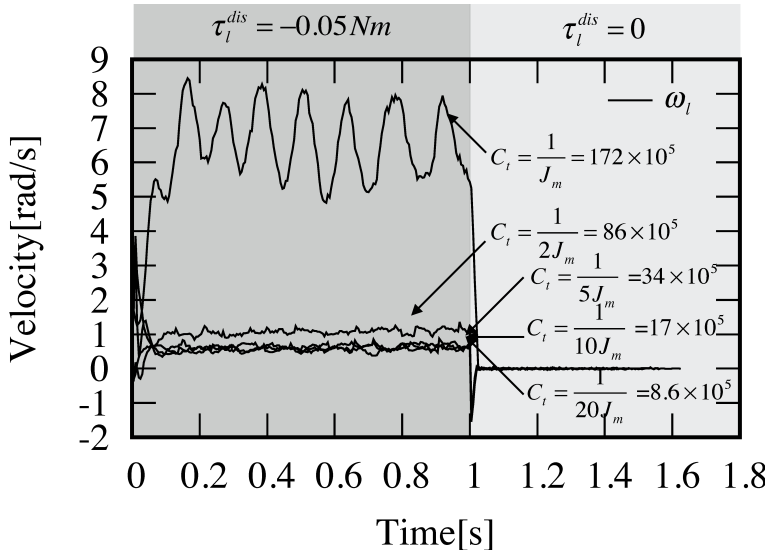

Fig. 45: Exp.1: velocity responses by increasing torque gain.

and proposed method. As we discussed about the effect of DOB before, the DOB not only compensates the modelling error and friction but also the torsional reaction torque from load side, which is performed as the motor impedance to reduce the velocity of motor output in

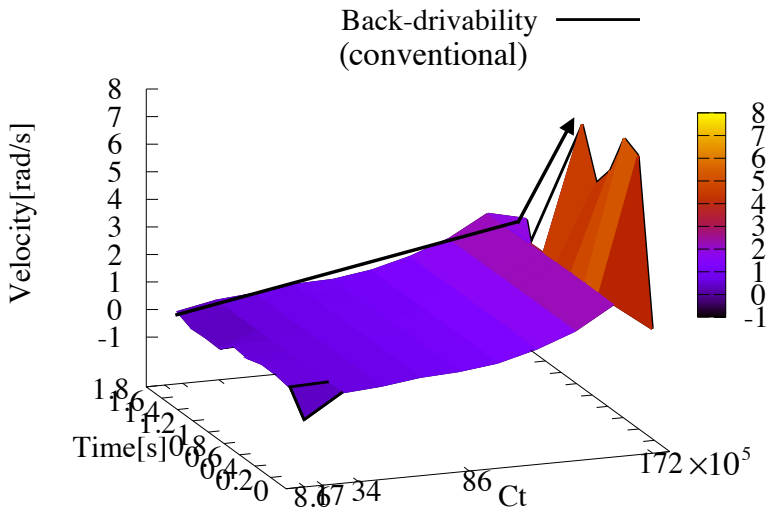

Fig. 46: Exp. 1: back–drivability by by torque gain.

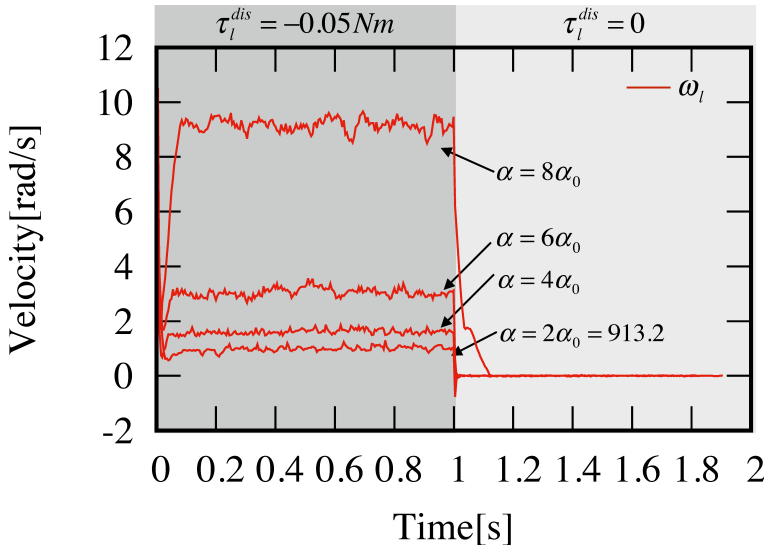

Fig. 47: Exp. 2: velocity responses by increasing scaling factor.

back–drive. The torque gain of torque feedback control is not proportional to back–drivability due to two terms of effect torques on the motor in opposite reaction. Only if the torque gain is selected big enough to overcome the other torque component, the back–drivability can not be shown as proportional. Furthermore, it is still not shown quantified improved in big gain due to big gain also lead to oscillation of output velocity. In proposed method, the scaling factor α is designed as the proportion of forward–drivability at the beginning. The two terms of effect torques on the motor in opposite reaction has been compensated by controller $H(s)$. In spite of the order difference in experiment according to the constructed strategy, the improvement of back–drivability of proposed method could realize quantified improvement by adjusting scaling factor.

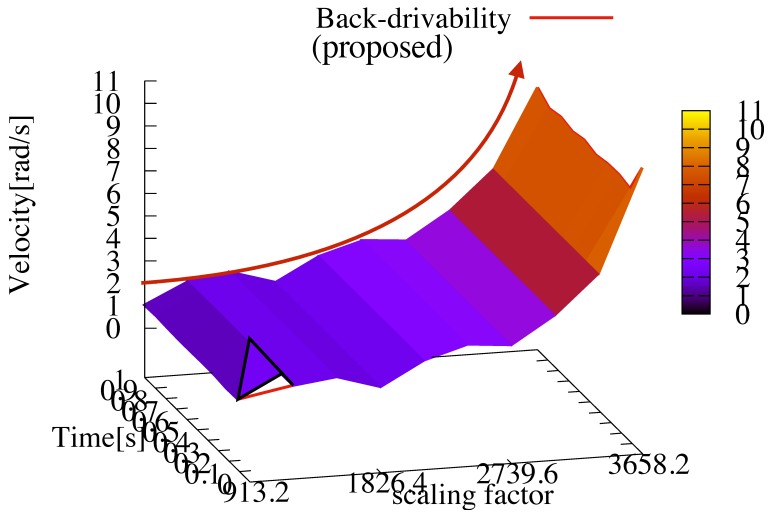

Fig. 48: Exp. 2: back–drivability by scaling factor.

Tab. 22: Comparison of referenced forward drive and proposed back drive in experiments.

Exp. 3	ω_m of referenced forward drive	$\tau_{cmd} = 0.05Nm(t \leq 1s)$
Exp. 4	ω_m of proposed back drive	$\tau_l^{dis} = -0.05Nm(t \leq 1s)(\alpha = 2\alpha_0)$

8.4 Experiment groups for referenced forward drive and proposed back drive

Groups of experiments related with referenced forward drive and proposed back drive are discussed in detail to show the relationship between the referenced forward drive and the constructed back drive completely.

8.4.1 Experiment of velocity responses

In chapter 5.4, the simulated results of referenced forward drive and proposed back drive had been shown. The results of both direction drives are given in the case as Tab. 22. In experiment results of Exp.3 and Exp.4 shown as Fig. 49, the scaling factor α is approximately selected as two times of α_0 to satisfy with the same scaling as referenced forward–drive. It is shown that the back–drivability realize almost 80 rad/s^2, while the forward–drivability is lower than simulated results (only around 60) rad/s^2, which are both lower than the simulate step responses in chapter 5.4. It is believed that this is due to model errors and friction that are not considered in the simulation.

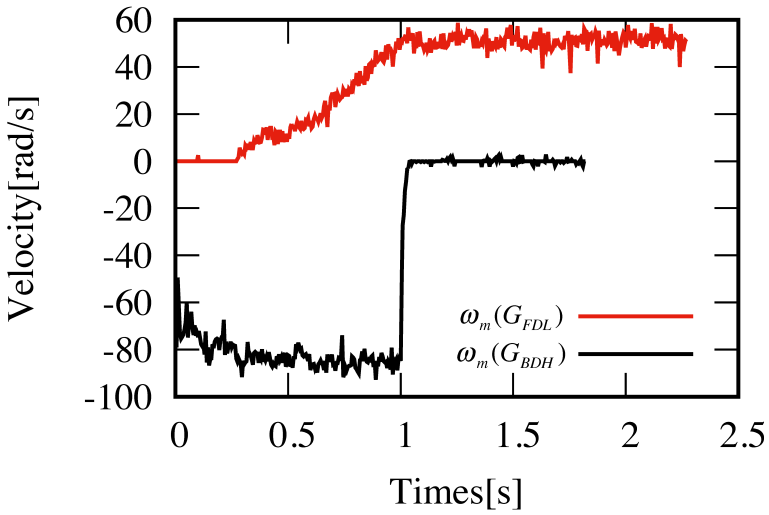

Fig. 49: Exp. 3, 4 : experimental comparison of forward–drivability and back–drivability in condition of $\alpha = 2\alpha_0$.

Tab. 23: Comparison of forward–drivability and back–drivability in different torque input.

Exp. 5	ω_m of referenced forward drive $0.3, 0.35, 0.4, 0.45Nm$	$\tau_{cmd} = 0.05, 0.1, 0.15, 0.2, 0.25,$
Exp. 6	ω_m of proposed drive $-0.3, -0.35, -0.4, -0.45Nm$	$\tau_l^{dis} = -0.05, -0.1, -0.15, -0.2, -0.25,$

8.4.2 Comparison according to input torque

A comparison of referenced forward drive and proposed back drive is given. A group of torque input for forward–drive and back–drive are given as Tab. 23. In this case, the scaling factor is assumed no α gain. As the construction of proposed back–drivability, the forward–drive and back–drive are supposed to achieve same amplitude and dynamic characteristic.

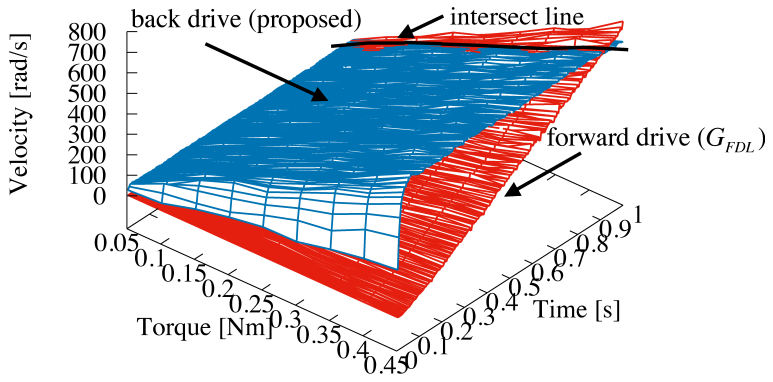

Fig. 50: Exp. 5, 6: comparison of forward–drivability and back–drivability.

Tab. 24: Limitation of scaling factor.

Exp. 7	$\tau_l^{dis} = -0.1Nm$	$\alpha = 8.26\alpha_0$

Fig. 50 is the figure of comparison of forward–drivability and back–drivability. The below curved surface is the increasing of velocities of motor in response to the growing of forward–drive input torque while the upper curved surface is it of back–drive input torque.

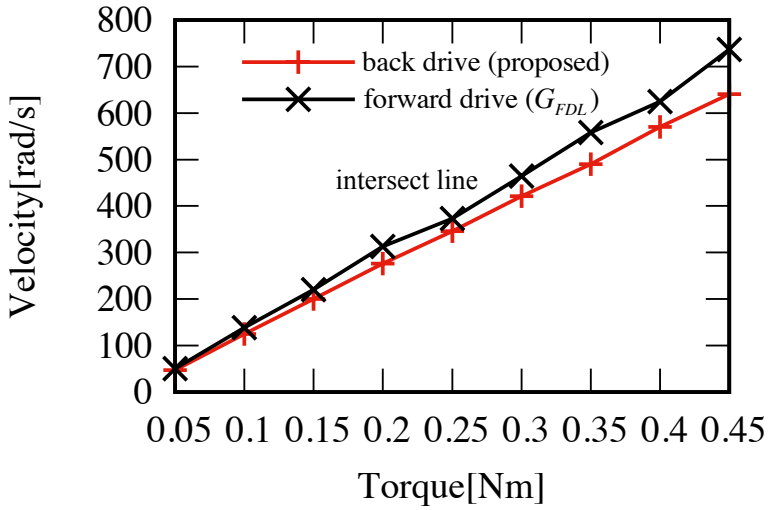

Fig. 51: Exp. 5, 6: the intersect line of forward–drivability and back–drivability.

From the conception of drivability which is given in chapter. 3, the included angle between coordinately plane to below surface is supposed to be the forward–drivability. In the same way, the included angle between coordinately plane to upper curve surface is the back–drivability. It is clear to see, the both two drivabilities are neither linear nor consistent to each other. However, there is a intersect line of two surface in somewhere and at some time shown as black line on the top of this figure. Fig. 51 is the intersect line of same drivability of forward–drive and back–drive at some time.

8.5 Limitation of α for improving back–drivability

Based on the reasons for the restriction on the value of α discussed in chapter. 7.3, the scaling factor $2\alpha_0$–$8\alpha_0$ is supposed to satisfied. Following case as Tab. 24 tries to discuss the performance of system with higher scaling factor than limitation.

The threshold value of $\alpha = 8.26\alpha_0$ is determined by trail and error to realize a better transient characteristics without overshoot and oscilation.

Fig. 52 shows the velocity of back drive and voltage of drive motor and load motor in condition

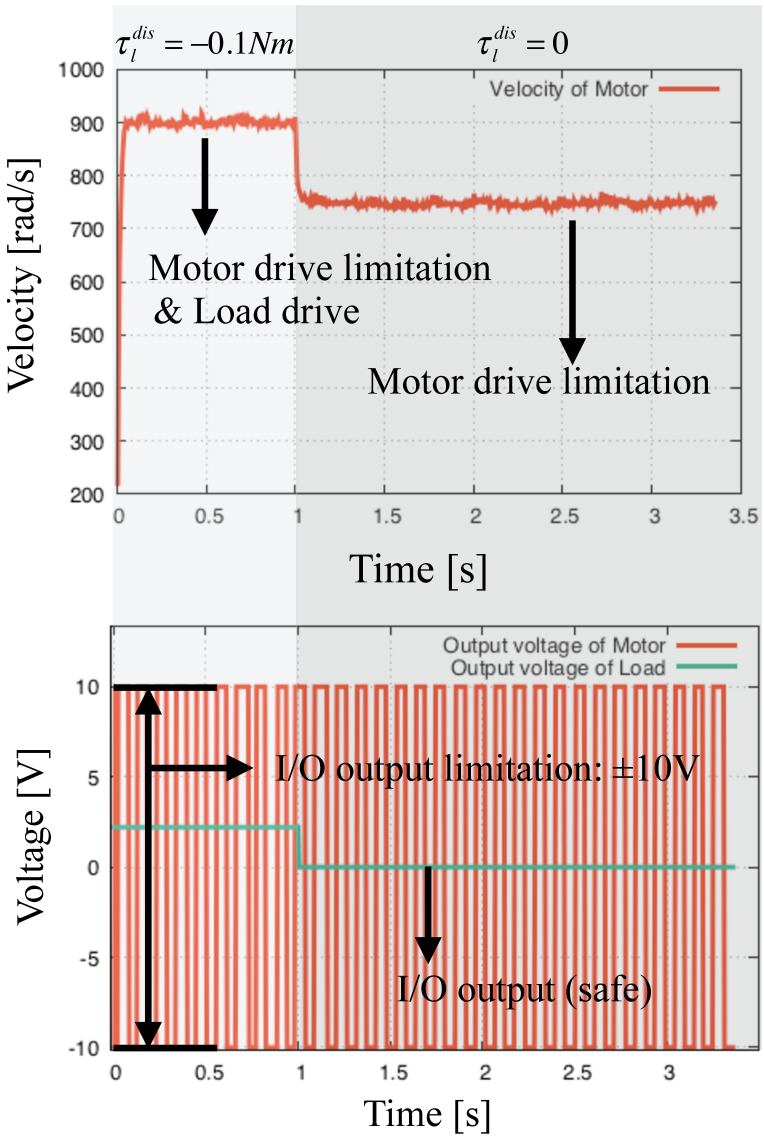

Fig. 52: Exp. 7: the threshold value of scaling factor.

of $\alpha = 8.26\alpha_0$.

The top half of Fig. 52 is the velocity response of proposed back drive. Within the time of being loaded with load torque, the system output velocity exceeds the upper limitation of the drive motor rad/s mentioned earlier as nearly 900, with the reason of the fact that the load motor also outputs torque to the system. At this point, the system is in a state where the controller is trying to get the drive motor to reach the desired velocity through designed controller, but is unable to achieve so due to the output voltage limitation of the I/O module ($\pm 10V$). When the external torque stops loading, the drive motor still gives the system the maximum output it can provide, which remains in the maximum speed operating state, since the previous control reference is not achieved.

It can be seen from the voltage diagram in the lower part, the system is in an uncontrollable state because the drive motor does not realize the velocity output required by the controller,

and the voltage oscillates between positive and negative maximums ($\pm 10V$), even after the external torque has disappeared. In the meantime, load motor is always in the safe output range, the output voltage returns to 0 after the external torque stops loading.

In summary, when the value of α is too large, the system will not be able to complete the required motion due to the hardware restriction. The improvement of back–drivability will be limited by the mechanical design of the system.

8.6 Summary of this chapter

In this chapter, related experiments of comparison evaluations with conventional method, the drivability comparison with referenced forward drive and back drive, and limitation of taking α are discussed to validate the conclusions of the various simulations performed in the previous chapters. Via the proposed method, back–drive can achieve the same level drivability as referenced forward–drive, and also can achieve quantified improvement of back–drivability by adjusting scaling factor under the limitation of mechanical design.

Chapter 9

Conclusion

In this thesis, a mechanical structure of a geared two–inertia system is introduced to be the model to discuss the conception of equivalent inertia from angular acceleration of motor to torque. The concept of back–drivability is also clarified in mathematics. Before presenting the proposed control strategy, the controller elements used in this thesis and a conventional torque control for back–drive are introduced. The characteristics of these components, which are based on the conventional method but are also used in later proposed method, are also described in detail to explain the advantages and reasons for using these control components. After those, the mathematic expression of performance of back–drivability is shown to evaluate progressive control results with step–by–step controllers based on referenced forward drive. A proposed semi–closed loop of torque control based on Disturbance Observe (DOB) and Load–side Disturbance Observer (LDOB) are implemented to geared two–inertia system to improve the back–drivability by three steps. A feedback controller is designed based on the target of estimation of forward–drive, in addition, the scaling α is also introduced to designed controller to make the performance of back–drivability adjustable.

Motion characteristics and frequency characteristics are discussed according to the expression of forward–drivability and back–drivability in both before and after the control design. In order to construct $H(s)$, many design parameters other than mechanical ones are introduced, such as g_{mdis}, g_{ldis}, g_{LPF} and α. The selection of these parameters can affect the stability and performance of the system. Since the take of α is not the same as the functional equation in a continuous system in a simulation and a discrete system in experiments, the identification of each of these parameters in different systems were validated by Root Locus Criterion, simulations and experiments results. The proposed control method was analysed based on both frequency characteristics and steady-state and transient responses.

Finally, in the experiment, the experimental setup of geared two–inertia system is describes in detail the experimental devices, as well as the hardware equipments. Related experiments of

comparison evaluations with conventional method, the drivability comparison with referenced forward drive and back drive, and limitation of taking α are discussed.

The proposed back drive control can get the desired results of back–drivability with simple controllers such as DOB, LDOB, and a construct feed–back controller based on a referenced forward drive. Without the complex mechanical design and high precision of parameter identification, the proposed back drive control can be applied to the wide range of applications to match different requests according to actual applications by adjustment of back–drivability.

Acknowledgment

I wish to thank everyone who helped me complete this thesis.

This research was supported in part by the New Energy and Industrial Technology Development Organization (NEDO) of Japan.

I would like to express my gratitude to my advisor, Prof. Shimono, for his support, patience, and encouragement throughout my graduate studies. He showed me the most important feature as a research is not how depth in one's researching field it is, but the strong desire and the power of taking action. It would be the wealth for me in the future whatever career I will go in for.

My thanks also go to Prof. Kawamura, Prof. Fujimoto, Dr. Motoi, Dr, Nozaki and so on who gave me the advises altruistically to my research in English Seminar and PEMC–camp. Their experiences and sensitivity of research field let me know how importance of the accumulation in study.

I got friendly treatment from graduated tutor Mr. Okubo and Mr. Morito who helped me to familiar with the new life in laboratory at the beginning since I came to Japan. Not mention other lab-mates like Mr. Togashi, Mr. Omura, Mr. Wada, and Mr. Ohori who gave me a lot of precious memories. And the sincere congratulation is given to the other international student Mr. Herman who will graduate from his Ph.D this year for good. Thanks for his sharing of experiences and proposals of living in abroad.

During these two and half years, also a lot of new members join us the big "Shimono Hotel" such as Mr. Tojo, Mr. Asai, Mr. Tanaku and Mr. Tanaka and so on. They make this "hotel" more lively than the time I just joined in. Since I am going to stay in this laboratory three years more for further education, wish to create something inconceivable in the future with all of you.

Thank you for everything.

Bibliography

[1] Suleiman Khayal, Osam, "Worm Gears". (2017)

[2] T. Kang, H. Kaminaga and Y. Nakamura, "A robot hand driven by hydraulic cluster actuators", *2014 IEEE-RAS International Conference on Humanoid Robots, Madrid*, pp. 39–44 (2014)

[3] Y. Kawai, Y. Katayama, and K. Ohishi, "Analysis of Back–drivability in Load–side Torque Control Based on New Index, *In Proceedings of 42nd Annual Conference of the IEEE Industrial Electronics Society*, pp. 6429–6434 (2016)

[4] G. A. Pratt, M. M. Williamso, "Series Elastic Actuator", *Proceedings 1995 IEEE/RSJ International Conference on Intelligent Robots and Systems*, Vol. 1 pp. 399–406 (1995)

[5] H. Asada, T. Kanade and I. Takeyama, "Control of a Direct-Drive Arm ", *Journal of Dynamic Systems, Measurement, and Control*, Vol. 105, pp. 136-242, (1983)

[6] G. Pratt, M. Williamson, P. Dillworth, J. Pratt, K. Ulland and A. Wright, "Stiffness Isn ' t Everything, " Preprints of the Fourth International Symposium on Experimental Robotics", (1995)

[7] T. Kawakami, K. Ayusawa, H. Kaminaga and Y. Nakamura, "High–Fidelity Joint Drive System by Torque Feedback Control Using High Precision Linear Encoder", *2010 IEEE International Conference on Robotics and Automation*, pp. 3904–3909 (2010)

[8] D.W. Robinson, "Design and Analysis of Series Elasticity in Close–Loop Actuator Force Control". *Ph.D. Thesis,* Massachusetts Institute of Technology, Cambridge, (2000).

[9] H. Vallery, J. Veneman, E. Asseldonk, R. Ekkelenkamp, M. Buss, H. Kooij, "Compliant Actuation of Rehabilitation Robot–Benefits and Limitations of Series Elastic Actuators". *IEEE Robot. Autom. Mag.*. vol. 15, pp. 60–69 (2008)

[10] M.J. Kim, W.K. Chung, "Disturbance–Observer–Based PD Control of Flexible Joint Robots for Asymptotic Convergence". *IEEE Trans. Robot.*vol. 31, pp. 1508–1516 (2015)

[11] N. Motoi, and K. Ohnishi, "Pushing Motion for Unknown Object by Humanoid Robot", *IEEJ Transactions on Industry Applications*, Vol. 128, No. 6 pp. 701–708 (2008)

[12] T. Nef, and P. Lum, "Improving Back–drivability in Geared Rehabilitation Robots", *Med Biol Eong Comput, Springer–verlag* 47,441 (2009)

[13] T. Yoshioka, A. Yabuki, Y. Yokokura, K. Ohishi, T. Miyazaki and T. T. Phuong, "Stable Force Control of Industrial Robot based on Spring Ratio and Instantaneous State Observer", *IEEJ Journal of Industry Applications*, Vol. 5, No. 2 pp. 132–140 (2016)

[14] Perret, Jerome and Vercruysse, Pierre. "Advantages of mechanical back–drivability for medical applications of force control". *Workshop on Computer/Robot Assisted Surgery (CRAS)* (2014)

[15] https://www.youtube.com/watch?v=33ojlV2hI6Q

[16] K. Nagasaka, Y. Kawanami, S. Shimizu, T. Kito, T. Tsuboi, A. Miyamoto, T. Fukushima and H. Shimomura, "Whole–body Cooperative Force Control for a Two–Armed and Two–Wheeled Mobile Robot Using Generalized Inverse Dynamics and Idealized Joint Units", *The 2010 IEEE International Conference on Robotics and Automation*, pp. 3377-3383. (2010)

[17] A. Albu–Schaffer, O. Eiberger, M. Grebenstein, S. Haddadin, Ch. Ott, T. Wimbock, S. Wolf and Gerd Hirzinger, "Soft Robotics: From Torque Feedback Controlled Lightweight Robots to Intrinsically Compliant Systems", *IEEE Robotics and Automation Magazine*, pp. 20-30, (2008)

[18] T. Kawakami, K. Ayusawa, H. Kaminaga and Yoshihiko Nakamura, "High-Fidelity Joint Drive System by Torque Feedback Control Using High Precision Linear Encoder", *Proceedings of 2010 IEEE International Conference on Robotics and Automation*, pp. 3904-3909, (2010)

[19] T. Wimbock, Ch. Ott, and G. Hirzinger, "Analysis and Experimental Evaluation of the Intrinsically Passive", *The 2008 IEEE International Conference on Robotics and Automation*, pp. 278-284 (2008)

[20] S. Ishikawa, M. Nishio and T. Sugihara, "Low–cost Back–drivable Motor Control Based on Feed–forward/Feed–back Friction Compensation", *IEEE International Conference on Robotics and Automation (ICRA)*, pp. 5027–5031 (2015)

[21] Y. Kawai, Y. Yokokura, K. Ohishi, K. Saito and A. Shimamoto, "High Back-Drivable Pseudo I-PD Torque Control Using Load-side Torque Observer with Torsion Torque

Sensor", *2016 IEEE 14th International Workshop on Advanced Motion Control (AMC)*, pp. 167–172 (2016)

[22] S. Yamada and H. Fujimoto, "Proposal of High Backdrivable Control Using Load–side Encoder and Backlash", *IEEE 42nd Annual Conference of the IEEE Industrial Electronics Society*, pp. 6429–6434 (2016)

[23] K. Yuki, T. Murakami and K. Ohnishi, "Vibration control of 2 mass resonant system by resonance ratio control," *Proceedings of IECON '93–19th Annual Conference of IEEE Industrial Electronics*", vol.3, pp.2009–2014 (1993)

[24] K. Ohnishi, M. Shibata, and T. Murakami, "Motion Control for Advanced Mechatronics", *IEEE/ASME Transactions on Mechatronics*, Vol. 1, No. 1 pp. 56–67 (1996)

[25] E. Sariyildiz, H. Yu, K. Yu and K. Ohnishi, "A nonlinear Stability Snalysis for the Robust Position Control Problem of Robot Manipulators via Disturbance Observer". *In Proceedings of the IEEE International Conference on Mechatronics (ICM)*, pp. 28–33 (2015)

[26] E. Sariyildiz, G. Chen, H. Yu, "An Acceleration–Based Robust Motion Controller Design for a Novel Series Elastic Actuator". *IEEE Trans. Ind. Electron.*, No. 63, pp. 1900–1910 (2016)

[27] E. Sariyildiz, K. Ohnishi, "Stability and Robustness of Disturbance–Observer–Based Motion Control Systems". *IEEE Trans. Ind. Electron.* vol. 62, pp. 414–422 (2015)

[28] S. Katsura, J. Suzuki, and K. Ohnishi, "Pushing Operation by Flexible Manipulator Taking Environmental Information into Account", *IEEE Transactions on Industrial Electronics*, Vol. 53, No. 5 pp. 1688–1697 (2006)

[29] H. Kobayashi, S. Katsura, and K. Ohnishi, "An Analysis of Parameter Variations of Disturbance Observer for Motion Control", *IEEE Transactions on Industrial Electronics*, Vol. 54, No. 6 pp. 3413–3421 (2007)

[30] Y. Kawai, Y. Yokokura, K. Ohishi, and P. Boonwong, "Analysis and Realization of Robot Actuator Based on Bidirectional Drivability Matrix", *Proceeding of the 20th World Congress of the International Federation of Automatic Control(IFAC2017 World Congress)*, pp. 12553–12558 (2017)

[31] M. Iwasaki, Y. Kitoh, and N. Matsui, "Analysis and Performance Improvement of Motor Speed Control System with Nonlinear Friction", *IEEJ Transactions on Electronics, Information and Systems*, Vol. 116–C, No. 1 pp. 96–102 (1996)

[32] T. Yoshioka, T. T. Phuong, A. Yabuki, K. Ohishi, T. Miyazaki and Y. Yokokura, “High–performance Load Torque Compensation of Industrial Robot using Kalman–filter–based Instantaneous State Observer”, *IEEJ Journal of Industry Applications*, Vol. 4, No. 5 pp. 589–591 (2015)

Presented Paper

Journal paper

[1] Shuang Xu, Minoru Yokohama, Shimono Tomoyuki: " Back–drivability Improvement of Geared 2–Inertia System Based on Disturbance Observer and Load–side Disturbance Observer", *IEEJ Journal of Industry Applications*, Vol.9, No.5, 2020

International Conference Paper

[1] Shuang Xu, Shimono Tomoyuki: " Modal MultirateControl for Scaled Bilateral System Taking Relative Velocity Resolution into Account" , *7th International Conference on Information and Automation for Sustainability, 2014* , 2014

Domestic Conference Paper

[2] Shuang Xu, Shimono Tomoyuki: " Performance Improvement Method Based on Moving Average for Micro Tele-manipulation" , *2013 IEE–Japan Industry Applications Society Conference, 2013*, 2013

[3] Shuang Xu, Minoru Yokohama, Shimono Tomoyuki: " Back–drivability Improvement of Geared 2–Inertia System Based on DOB and LRTOB" , *IEE–Japan Mechatronics Control, 2017*, 2017

[4] Shuang Xu, Minoru Yokohama, Shimono Tomoyuki: " Back–drivability Improvement of Geared 2–Inertia System Based on Disturbance Observer and Load–side Disturbance Observer" , *2018 IEE–Japan Industry Applications Society Conference, 2018*, 2018